Bright and dark regions on Mars: Particle size and mineralogical characteristics based on Thermal Emission Spectrometer data

Steven W. Ruff and Philip R. Christensen

Mars Space Flight Facility, Department of Geological Sciences, Arizona State University, Tempe, Arizona, USA

[1] Emissivity spectra (1670–200 cm^{-1}) from the Mars Global Surveyor Thermal Emission Spectrometer (MGS-TES) show significant differences between bright and dark surfaces, allowing further investigation of their physical and mineralogical character. TES spectra from bright surfaces (albedo $\geq$0.2) typically show lower emissivity at high wavenumbers (>1300 cm^{-1}) than that of dark surfaces (albedo <0.2). The opposite behavior is evident in the low wavenumbers (<560 cm^{-1}), where bright surfaces have higher emissivity than dark ones. These trends are consistent with the spectral behavior of silicate materials of varying particle size. The short wavelength feature displayed by TES spectra of bright surfaces is a relatively strong absorption that likely is the result of particle size effects of surface silicate particles $\ll$100 μm in size. A dust cover index (DCI) is developed that exploits this short wavelength feature, serving to identify surfaces that range from dust-covered to dust-free. As a gauge of surface-obscuring silicate dust that can impact spectral measurements, the DCI is more direct than thermal inertia or albedo measurements. Spectral ratio analysis using emissivity spectra from adjacent bright and dark surfaces is explored as a means of deriving the mineralogy of surface dust. The result shows that the dust is dominated by silicate minerals with indication of a significant plagioclase feldspar component. *INDEX TERMS:* 5410 Planetology: Solid Surface Planets: Composition; 5464 Planetology: Solid Surface Planets: Remote sensing; 5470 Planetology: Solid Surface Planets: Surface materials and properties; 5494 Planetology: Solid Surface Planets: Instruments and techniques; 6225 Planetology: Solar System Objects: Mars; *KEYWORDS:* Mars, dust, infrared, albedo, TES

Citation: Ruff, S. W., and P. R. Christensen, Bright and dark regions on Mars: Particle size and mineralogical characteristics based on Thermal Emission Spectrometer data, *J. Geophys. Res.*, *107*(E12), 5127, doi:10.1029/2001JE001580, 2002.

1. Introduction

[2] Visibly bright and dark regions on Mars have long been recognized, first by astronomers and more recently, by investigators using instruments on spacecraft. The origin of these features was the subject of considerable controversy, with the possible role of vegetation being debated into the late 1960s [*Salisbury*, 1966; *Adams and McCord*, 1969; *Sagan and Pollack*, 1969]. Although the vegetation debate has mostly subsided, global remote-sensing investigations of the physical and mineralogical nature of bright and dark surface features have continued. The generalized view that has emerged is that classical bright features are regions covered by a layer of dust [*Kieffer et al.*, 1973, 1977] up to 2 m thick with particles in the size range of 2–40 μm [*Christensen*, 1986]. The classical dark features are relatively dust-free but are still dominated by particulate materials ranging from 0.1 mm to 1 cm [*Christensen and Moore*, 1992] rather than bedrock. Compositionally, dark regions appear to be dominated by minerals found in mafic volcanic rocks, specifically, pyroxene [e.g., *Singer et al.*, 1979; *Mustard et al.*, 1993; *Bell et*

al., 1997; *Bandfield et al.*, 2000a; *Christensen et al.*, 2000a] and plagioclase [*Bandfield et al.*, 2000a; *Christensen et al.*, 2000a]. The mineralogy of bright-region dust is not fully resolved but there is some consensus that palagonite, an alteration product of mafic volcanic glass, is a significant component [e.g., *Singer*, 1982; *Bell et al.*, 1993; *Morris et al.*, 2001].

[3] With the advent of the Mars Global Surveyor Thermal Emission Spectrometer (TES) [*Christensen et al.*, 1992, 2001], it is now possible to examine the thermal-infrared (TIR) spectral character (~1670–200 cm^{-1}) of Mars at a combined spatial and spectral sampling (3 × 6 km and 10 cm^{-1}, respectively) previously not available. To date, surface studies using TES spectra have focused on dark regions, where basalt, basaltic andesite, and hematite-rich materials have been identified [*Bandfield et al.*, 2000a; *Christensen et al.*, 2000a, 2000b]. Although a linear deconvolution method for surface-atmosphere separation is employed in those studies [*Smith et al.*, 2000a], this method has limitations for examining the spectral characteristics of bright regions. Specifically, the method excludes the high wavenumber region of TES spectra and incorporates the assumption that bright regions have no spectral features. The purpose of this paper is to contrast the spectral characteristics of bright and dark
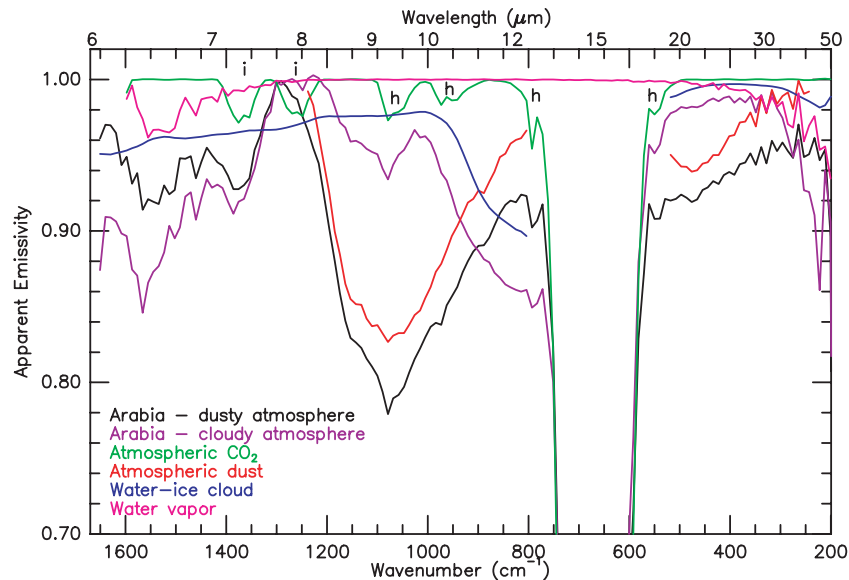
Figure 1. Demonstration of the appearance of atmospheric spectral features in TES spectra and in isolation. The two TES spectra, which are the average of 120 individual spectra from a common location in Arabia Terra (see Figure 5 for data details), show the dramatic variations that result from different atmospheric conditions. The spectra of the atmospheric components shown in isolation are modeled results (see text for details). The letter h indicates a CO_2 hot band and the letter i indicates a CO_2 isotope band. All spectra are displayed with 10 cm^{-1} sampling.

regions which are here defined loosely by their broadband visible to near IR (0.3–3.0 μm) lambert albedo values where bright is ≥0.2 and dark is <0.2. The classical bright and dark features of Mars that have been known for centuries from telescopic observations fit this definition and provide a logical basis for comparison. We will demonstrate that: (1) surface spectral information is discernable without surface-atmosphere separation, (2) bright regions have an important and useful absorption feature at high wavenumbers (>~1300 cm^{-1}), (3) major TIR spectral differences between bright and dark regions are due to particle size effects, and (4) carefully applied ratios of spectra from bright and dark surfaces produce features attributable to surface dust.

[4] Because the spectral features of the atmosphere are so significant, section 2 describes the identification of such features in TES spectra. In section 3, the spectral differences between bright and dark regions are shown and compared under varying atmospheric conditions. The relationship between these spectral differences and the particle size and mineralogy of surface materials is described in section 4 followed by the development of a dust cover index (DCI) based on high wavenumber emissivity in section 5. Finally, our results will be discussed in section 6 and conclusions given in section 7.

## 2. Spectral Features of the Atmosphere

[5] Thermal-IR spectra of Mars are dominated by atmospheric absorptions. In order to distinguish the spectral features of the surface from those of the atmosphere, it is necessary first to recognize the multitude of atmospheric features. Figure 1 shows two TES spectra that display the combined features of atmospheric CO_2 gas, dust, water vapor, and water ice. The modeled spectra of individual atmospheric components shown with the same 10 cm^{-1} sampling as the TES spectra are included.

[6] All the TES spectra in this paper are plotted as apparent emissivity versus wavenumber. The measured spectrum has been calibrated to radiance and then divided by a Planck curve at the maximum brightness temperature calculated from the radiance spectrum. In this form, primary temperature effects are removed. For convenience, spectra of the atmospheric components shown in Figure 1 are also plotted with units of apparent emissivity rather than the more common use of brightness temperature or opacity [e.g., *Smith et al.*, 2000a].

2.1. Carbon Dioxide Gas

[7] The CO_2 spectrum in Figure 1 was supplied by J. Pearl and G. Bjoraker (personal communication), produced with a line-by-line, layer-by-layer technique based on the work of *Kunde and Maguire* [1974]. The following conditions were applied: the atmospheric temperature profile was 260 K at surface level (6.1 mbar surface pressure), decreasing 3 K km^{-1} with altitude to 300 km, where it becomes isothermal; the surface temperature was 300 K. Several CO_2 absorptions are evident throughout the TES spectral range (for detailed studies see works of *Maguire* [1977], *Crisp* [1990] and *Rothman* [1992]). Most dominant is the one centered at 667 cm^{-1} (15 μm) arising from the fundamental bending mode of gaseous CO_2. Although it appears as a single feature in a TES spectrum, additional CO_2 bands related to rotation-vibration coupled modes, CO_2 isotopes, and Fermi resonances produce the observed shape [e.g., *Goody and Yung*, 1989]. The opacity of this
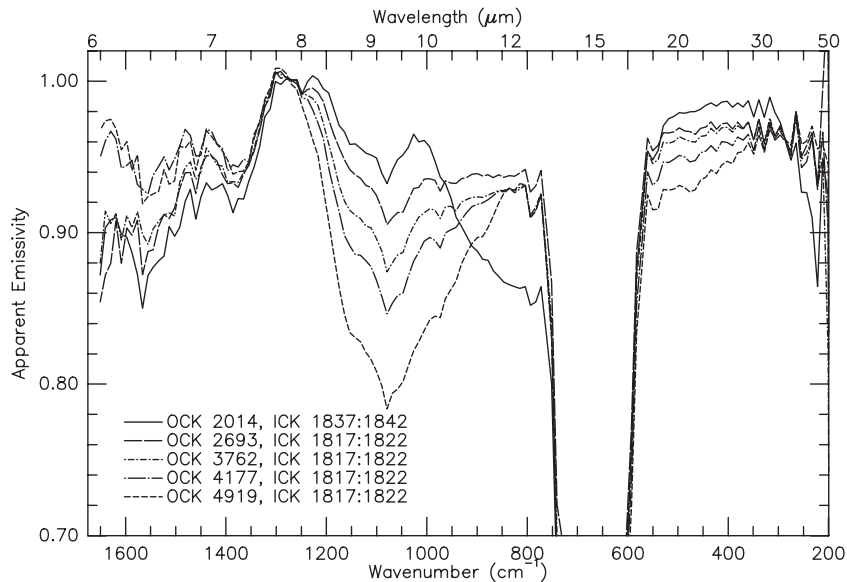
Figure 2. Spectral changes that accompany the variation of water-ice cloud and aerosol dust opacity over a location in Arabia Terra. The solid line is from a cloudy period with low dust concentration and the dashed line is from a very dusty, effectively cloud-free period. OCK is the TES orbit indicator and ICK is the incremental observation counter.

feature at its center is so high that surface radiance is completely absorbed and thus does not reach an orbiting instrument. For a typical daytime TES spectrum, the surface radiance component only becomes significant at $>\sim780$ and $<\sim560$ cm^{-1}.

[8] Outside of the 667 cm^{-1} CO_2 feature is a set of "hot bands", which are absorptions that arise from vibrational transitions originating from above the ground state. Two notable hot bands are readily apparent on either side of the 667 cm^{-1} feature, one at ~544 cm^{-1} and the other at ~790 cm^{-1} (Figure 1). A pair of weak doublets, one centered at ~960 cm^{-1} and the other at ~1060 cm^{-1} also are hot bands [e.g., *Maguire*, 1977]. These are less discernable in TES spectra because they overlap with the prominent aerosol dust and water-ice absorptions. Hot band absorptions are very sensitive to temperature, increasing in intensity with increasing atmospheric temperature.

[9] A final set of CO_2 features arises from the various isotopes of oxygen and carbon that can be found in the molecule. Most significant for TES spectra are the weak doublets centered at ~1260 and 1365 cm^{-1} that are the result of a Fermi resonance between fundamental modes of the $^{18}O^{12}C^{16}O$ isotope [*Young*, 1982]. Compared with hot bands, these absorptions are much less sensitive to the temperature of the atmosphere.

2.2. Aerosol Dust

[10] The atmosphere of Mars is never free from dust although seasonal variability is well documented (most recently by *Clancy et al.* [2000] and *Smith et al.* [2000b]). Because the dust is such a strong absorber, it results in the next most prominent feature in TES spectra relative to CO_2. Centered at ~1075 cm^{-1} (~9 μm), aerosol dust produces a prominent V-shaped absorption that is accentuated by the presence of a CO_2 hot band

roughly at the center of the trough [*Hanel et al.*, 1972; *Conrath et al.*, 1973]. The V-shape is relatively symmetric but becomes increasingly asymmetric when combined with a water-ice absorption. On the low wavenumber side of the 667 cm^{-1} CO_2 feature, atmospheric dust has another absorption centered at ~470 cm^{-1} as shown by the modeled dust spectrum in Figure 1. This spectrum is from the work of *Bandfield et al.* [2000b] but has been modified by dividing out water vapor and CO_2 hot bands using the spectra shown. Such a modification is not rigorously correct, but gives a qualitative look at the dust spectral shape in the absence of major atmospheric gas absorptions. The spectral region >1300 cm^{-1} was not included in the work of Bandfield et al. However, it has been shown previously that atmospheric dust is relatively transparent and spectrally featureless in this region [e.g., *Toon et al.*, 1977], which is demonstrated further in section 4.

2.3. Water-Ice Clouds

[11] The occurrence of water-ice clouds and hazes is highly variable in space and time [e.g., *Beish and Parker*, 1990; *Bell et al.*, 1996; *Pearl et al.*, 2001]. Water ice has a deep and relatively broad absorption centered at ~825 cm^{-1} and a narrower absorption at ~230 cm^{-1} [*Curran et al.*, 1973] (Figure 1). Figure 2 shows a series of spectra from the same geographic location in Arabia Terra from early summer to late fall (L_s, $120°-253°$) during which time water-ice clouds give way to atmospheric dust. Dramatic spectral changes accompany this atmospheric transition, most notably in the $800-1250$ cm^{-1} range.

2.4. Water Vapor

[12] Figure 1 shows a water vapor spectrum modeled using 10 precipitable microns of water and the same
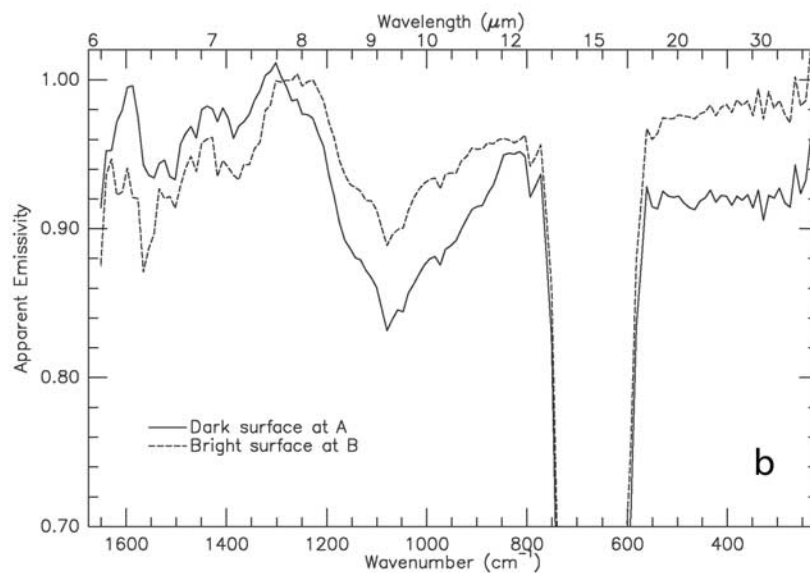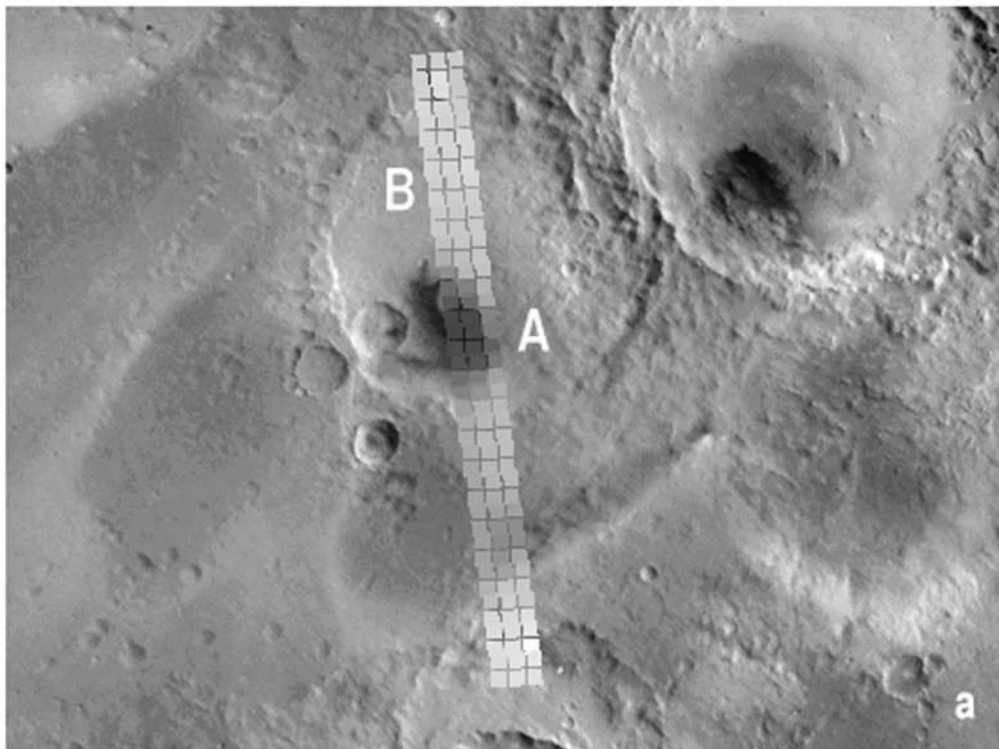
Figure 3. Comparison of spectra from adjacent bright and dark surfaces. (a) A dark splotch on the bright floor of an unnamed crater in western Arabia at 11°N, 348°W showing albedo for a segment of a TES ground track from OCK 3461, ICK 1840−1860. (b) The average spectra from 8 dark pixels at A (ICK 1851, det. 1:3, 5, 6 and ICK 1852, det. 2, 3, and 6) and 12 bright pixels at B (ICK 1856−57, all detectors) show clear differences that are attributable to variations of surface emissivity.

technique used to model CO_2 described in section 2.1. Water-vapor concentration in the Martian atmosphere is variable in space and time but is in the range of a few to several tens of precipitable microns [e.g., *Jakosky and Farmer*, 1982; *Clancy et al.*, 1996]. The concentration of Martian water vapor is never sufficient to produce deep absorption features but numerous shallow, narrow features exist in the spectral regions >1400 and <500 cm^{-1}. At wavenumbers >1400 the absorptions are due to the fundamental bending mode vibration and coupled rotation-vibration modes of the H_2O molecule while those at low wavenumbers (<500) are due to molecular rotations. In both cases, many individual absorptions are narrower than the 10 cm^{-1} (or even 5 cm^{-1}) spectral sampling of the TES
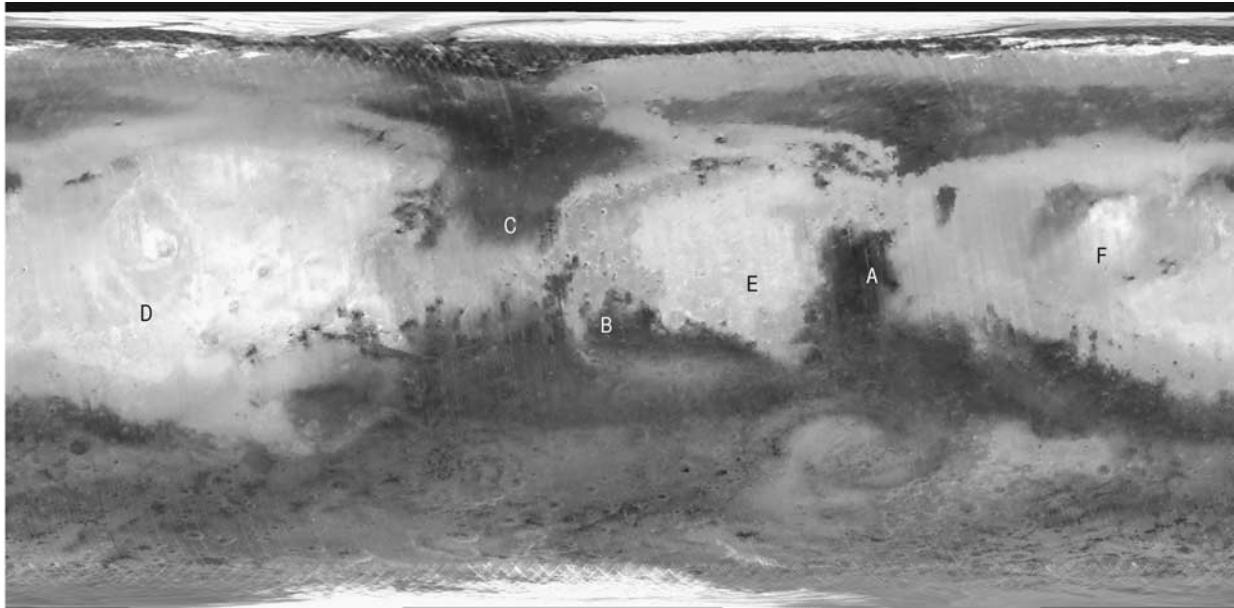
Figure 4. Location map of bright and dark regions of interest. TES-derived global lambert albedo is shown with letters indicating the following locations: A, Syrtis Major; B, Sinus Meridiani (hematite-rich area); C, Acidalia; D, Tharsis; E, Arabia; and *F*, Elysium.

instrument. The end result is a sawtooth appearance in the water-vapor regions of TES spectra (Figure 1).

3. Bright and Dark Region Spectral Differences

[13] TES spectra can yield useful information about the Martian surface even in the absence of surface-atmosphere separation. A clear demonstration is provided by comparing bright and dark surfaces that are adjacent to one another using spectra from the same orbit. The dark splotches on the bright floors of many craters in western Arabia Terra/Oxia Palus offer an ideal opportunity for examining bright/dark spectral differences at a very local scale. Figure 3a shows one such example where dark material is directly adjacent to bright material on the floor of an unnamed crater in western Arabia. Eight spectra were averaged from the dark surface (average albedo of ∼0.12) and 12 from the bright surface (average albedo of ∼0.26) just to the north; the result is shown in Figure 3b. Variations in the atmosphere are assumed to be minor given the close proximity of these surfaces both in lateral distance (∼30 km apart) and in elevation (∼200 m apart). Therefore, the most significant differences between the two spectra are due to surface emissivity variations. In this example, the dark-surface spectrum has deeper features than the bright-surface spectrum in the ∼1300−780 and ∼560−200 cm^{-1} ranges. This character is reversed for the spectral range >∼1300 cm^{-1}, where the bright-surface spectrum has deeper features. Sections 3.1−3.4 demonstrate that these characteristics persist at a global scale and under a range of atmospheric conditions.
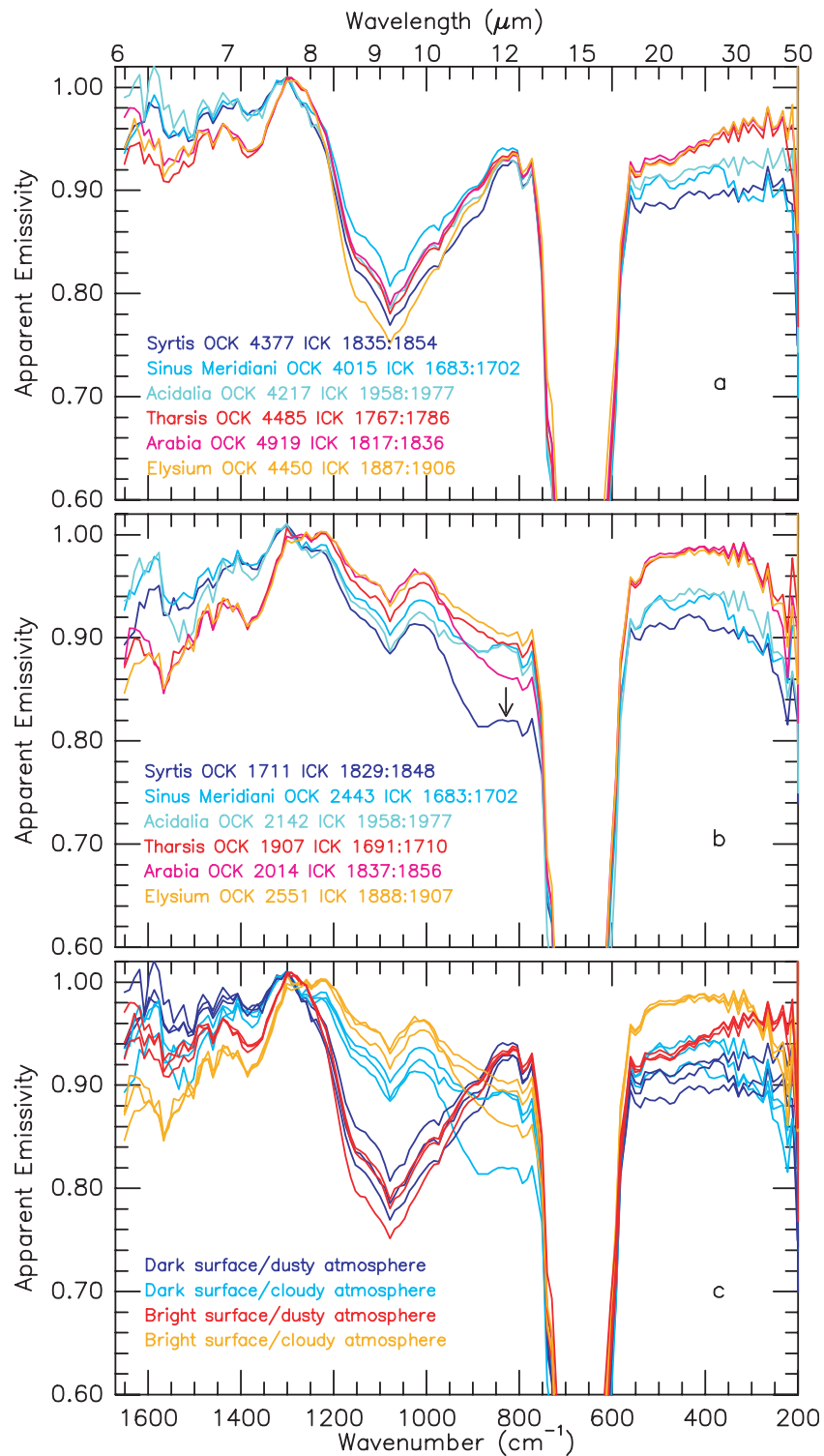
3.1. Regions of Interest

[14] Small portions of three bright regions (Arabia Terra, Tharsis Montes, and Elysium Planitia) and three dark regions (Syrtis Major Planum, Sinus Meridiani, and Acid-

alia Planitia) as shown in Figure 4 were selected for detailed spectral analysis. The TES instrument has viewed ∼90% of the planet from mapping orbit throughout the course of a full Martian year. Therefore observations exist for the same or nearby regions (<10 km distant) under very different atmospheric conditions. For this study, spectra from the selected regions of interest were chosen to maximize the extremes of atmospheric dust and water-ice clouds with the intent of bracketing the possible range of atmospheric spectral variations (excluding dust storms). Additional selection criteria included a search for the highest surface temperatures for a given region, to improve the signal-to-noise ratio (SNR), and dusty/cloudy orbits that spatially overlapped each other as much as possible.

[15] To further enhance spectral SNR, 20 ICKs (TES incremental observation counter) of all six detectors were averaged for each region of interest (120 total spectra). The center detector *x* axis data were used for all spectra to allow averages to be calculated conveniently. Twenty ICKs in mapping orbit cover a ground swath of ∼120 km in latitude and 9 km in longitude. This area is small enough to avoid any major spectral variations on the surface of the regions of interest (verified by inspection of each spectrum) but large enough to produce a high SNR. Complete latitudinal overlap of the dusty/cloudy orbit pair for each region was available while longitudinal overlap of at least 1/3 of the orbit pair was possible.

3.2. Bright/Dark Differences: Dusty Atmosphere

[16] Figure 5a shows spectra of the six regions of interest viewed through a dusty atmosphere. The prominent, nearly symmetrical V-shaped atmospheric dust absorption dominates the 800−1300 cm^{-1} range. Any differences between bright and dark surfaces from 800 to 1300 cm^{-1} are obscured by the variation in intensity of the atmospheric dust feature. This is not the case outside of this spectral

Figure 5. Averaged spectra from six bright and dark regions of interest. Figure 5a shows spectra (identified using TES orbit counter and increment counter designations) obtained under very dusty atmospheric conditions while those in Figure 5b had diminished dust but significant water-ice cloud conditions during measurement (arrow indicates feature described in section 3.3). Figure 5c shows the spectra from Figures 5a and 5b combined to allow the direct comparison of emissivity for both atmospheric conditions. These plots form the basis for comparison of the spectral characteristics of Martian bright and dark regions.

range. At wavenumbers >1300 and <560, the bright and dark surfaces are spectrally separable. The bright-surface spectra (red shades in Figure 5a) display higher emissivity at low wavenumbers than the dark-surface spectra (blue shades). This behavior is reversed at the high wavenumber end where the bright targets have lower emissivity. Also noteworthy is the observation that among the dark-surface spectra, there is significant variation in emissivity in the <560 cm^{-1} range, an indication of varying surface mineralogy. In the >1300 cm^{-1} range, dark-surface spectra show no significant variation. Among the bright-surface spectra there is no significant variation in either the high or low spectral range, an indication that these bright surfaces have similar composition and particle size.

3.3. Bright/Dark Differences: Cloudy Atmosphere

[17] In the presence of abundant water-ice clouds, the depth of the ~1075 cm^{-1} atmospheric dust feature typically is significantly reduced and the water-ice feature centered at ~825 cm^{-1} is clearly evident (Figure 5b). Because of the reduced intensity of the atmospheric dust feature it is possible to see that dark surfaces have lower emissivity than bright surfaces, at least in the range from 1300 to ~1000 cm^{-1}. From ~1000 to 780 cm^{-1}, dramatic changes in apparent emissivity occur as the concentration of water-ice aerosols varies in time (Figures 5a and 5b). Figure 6 demonstrates that cloud features can also vary over small spatial scales. Nevertheless, evidence of a spectral distinction between bright and dark surfaces is present in the form of an upturn in emissivity centered at ~825 cm^{-1} that creates a flattened local maximum in dark-surface spectra (arrow in Figure 5b). This is not the case with bright surfaces; a local minimum is observed whose low wavenumber side is lost in the 667 cm^{-1} CO$_2$ feature. These characteristics are also evident in Figure 6.

[18] In the low wavenumber range (<560 cm^{-1}) spectra from bright and dark surfaces display a clear separation of emissivity, but the combined effects of reduced dust concentration and increased water-ice and water-vapor concentration modifies the apparent emissivity from that observed in the dusty atmosphere case. Most significant is a downturn in emissivity in the lowest wavenumbers attributable to absorptions from both H$_2$O components. At high wavenumbers (>1300 cm^{-1}), water-ice absorption reduces the apparent emissivity of both bright- and dark-surface spectra, but the emissivity separation between the two groups remains.

3.4. Bright/Dark and Dusty/Cloudy Direct Comparison

[19] Because bright and dark surfaces have spectrally distinct characteristics, it should be possible to map these differences on a global scale using the full TES data set. However, first it must be shown that the emissivity characteristics outlined above persist in an absolute sense regardless of atmospheric conditions. Figure 5c combines the spectra from Figures 5a and 5b. In this way the emissivity characteristics of bright and dark surfaces can be examined under the full range of atmospheric conditions (excluding dust storms). It is evident from this figure that the high and low wavenumber separation in the apparent emissivity of bright and dark surfaces is retained in the presence of atmospheric variations for portions of the TES spectral

range. In particular, the ranges from 1300 to 1400 cm^{-1} and from ~250 to 400 cm^{-1} show good separation. The causes of these spectral differences is investigated in the following section.

4. Origins of Bright and Dark Region Emissivity Characteristics

[20] The IR spectral character of geologic materials is a function of both composition and particle size. In an effort to understand the observed emissivity differences between bright and dark regions and to investigate the composition of bright dust, it is necessary to examine the relationship between emissivity and both particle size and composition.

4.1. Particle Size Effects

[21] The changes to thermal-IR spectra resulting from variations in particle size have long been recognized and modeled [e.g., *Lyon*, 1965; *Hunt and Vincent*, 1968; *Conel*, 1969; *Emslie and Aronson*, 1973; *Salisbury and Wald*, 1992; *Moersch and Christensen*, 1995; *Wald and Salisbury*, 1995; *Ramsey and Christensen*, 1998; *Lane*, 1999]. From such studies it has been established that spectral contrast (amplitude of features) decreases in particulate samples compared with their solid form due to the increase in porosity and accompanying incoherent scattering of light from multiple surface reflections. With decreasing particle size, the diameter approaches a critical limit below which new spectral features arise. Wherever the absorption coefficient (k) of the material is very low and the index of refraction (n) is close to but greater than unity (a transparency region), light can interact with many more particles to produce an absorption feature. Both single minerals and mineral mixtures display surface scattering and volume scattering or transparency features (Figure 7). The size at which particles begin to display transparency features varies widely depending on composition and wavelength. For example, carbonates begin to show such features for particles in the range of 500–710 μm [*Lane and Christensen*, 1998] while silicates do not begin to show them until particles are less than ~100 μm [e.g., *Moersch and Christensen*, 1995].

[22] The impact of particle size effects on thermal-IR spectra measured from planetary surfaces has been a focus of concern for decades. The spectral contrast of fundamental mode absorption features (reststrahlen bands) is reduced for small particles making these features more difficult to detect. However, features related to volume scattering have been recognized as potentially useful for remote sensing of planetary surfaces because of their prominence [*Salisbury et al.*, 1987; *Salisbury and Walter*, 1989]. Transparency features (TF in Figure 7) commonly occur in the weakly absorbing, intraband regions between the strongly absorbing, fundamental mode absorptions [*Vincent and Hunt*, 1968; *Conel*, 1969; *Salisbury and Walter*, 1989; *Moersch and Christensen*, 1995] but are not limited to these regions [*Salisbury et al.*, 1987; *Lane*, 1999]. *Salisbury and Walter* [1989] demonstrated that a transparency feature in the 11–13 μm (~910–770 cm^{-1}) spectral region of powdered igneous rocks (≤74 μm) is related to composition. However, *Mustard and Hays* [1997] observed changes in the position and shape of transparency features with decreasing
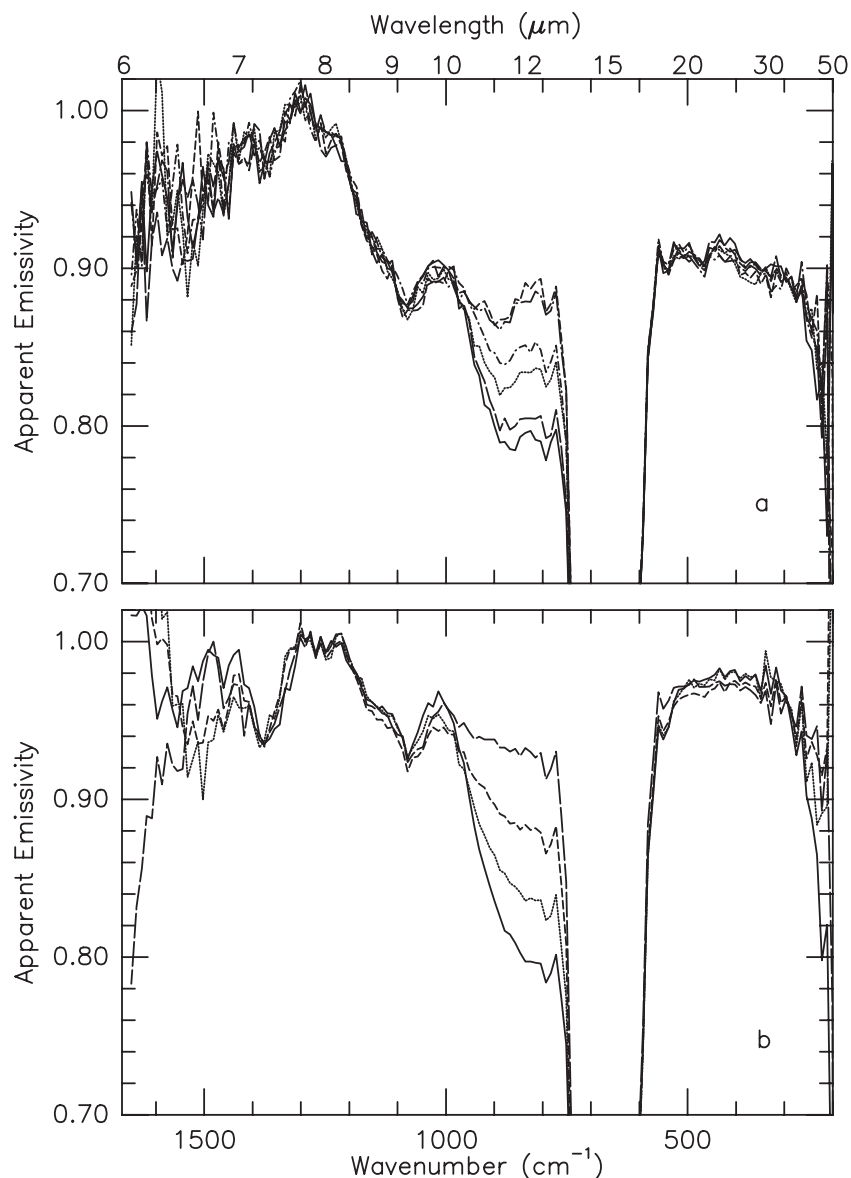
Figure 6. Demonstration of the variability of water-ice cloud features ($\sim$825 and $\sim$230 cm^{-1}) over small spatial scales for a dark and bright location. (a) A single TES ICK from Syrtis Major (centered on 10.9°N, 289.0°W) showing cloud variability between the six detectors (OCK 1711, ICK 1846). (b) A set of spectra spanning 1.3° of latitude in Elysium Planitia (centered on 31.2°N, 216.0°W); each spectrum is a six-detector average from OCK 2073, ICK 2045, 2048, 2054, and 2058. Note the difference in shape of the $\sim$825 cm^{-1} cloud feature for a dark surface (Figure 5a) versus a bright surface (Figure 5b) that results from surface emissivity.

particle size, which is also evident in the central transparency feature of the andesine (An$_{48}$) in Figure 7a. Although these observations do not rule out the utility of transparency features for compositional assessment, they do indicate the need for caution when interpreting them.

[23] A prominent transparency feature is found at wave numbers greater than the principal Christiansen feature (the emissivity maximum defined as the location in a spectrum where n is near unity and k is low (<0.1) [*Conel*, 1969]). In some cases, narrow peaks are superimposed on this feature. These have been attributed to overtones or combination tones of the fundamental mode vibrations at lower wavenumbers [*Salisbury et al.*, 1987, 1991; *Salisbury and*

Walter, 1989]. Their visibility in the spectra of fine-particulate materials has been explained as a combination of surface scattering and volume scattering effects [*Salisbury et al.*, 1987]. While the value of these overtone and combination tone features for remote sensing of particulate planetary surfaces has been advocated, the broad transparency feature on which they are superimposed can be a useful indicator for the presence of fine particulates.

4.2. Evidence for Silicate-Related Particle Size Effects in TES Spectra

[24] The evidence for particle size effects in TES spectra is most apparent when bright and dark regions are compared
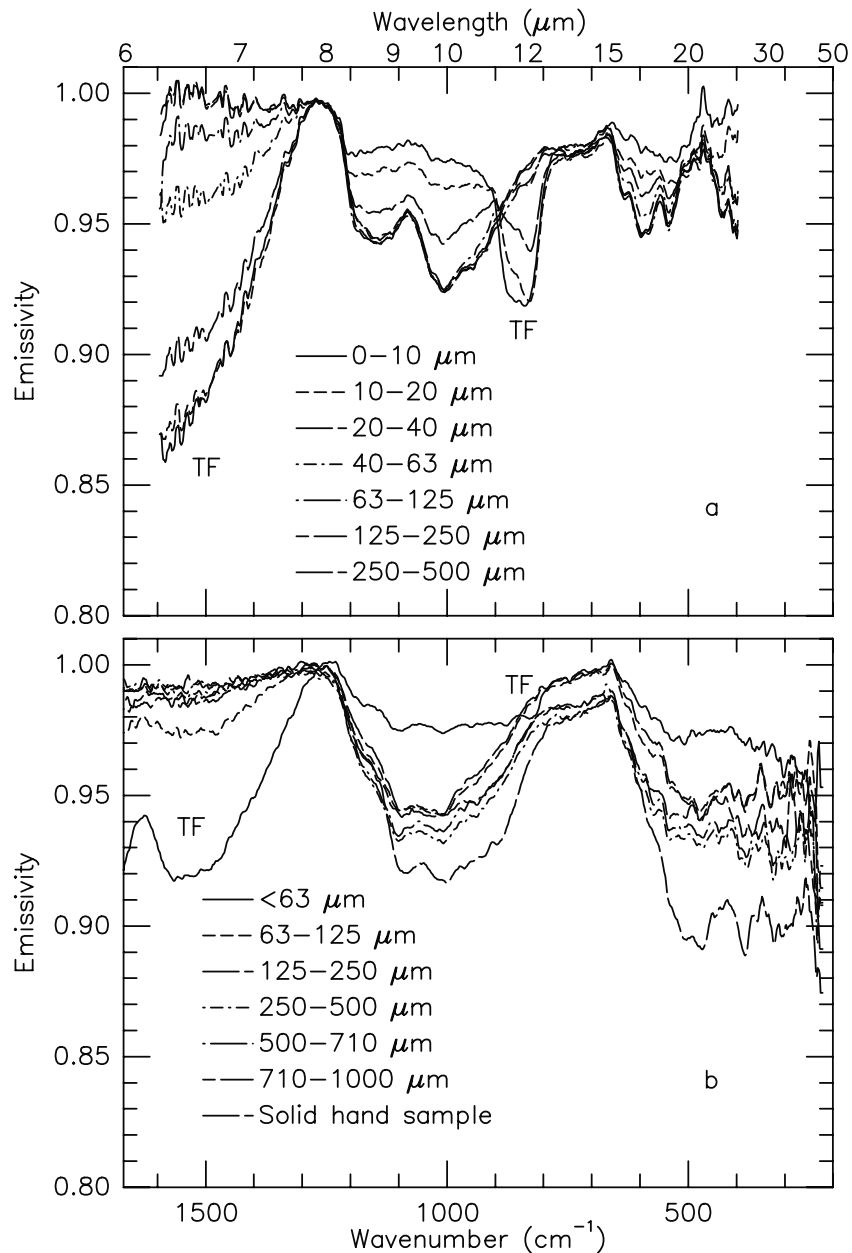
Figure 7. Example of spectral particle size effects for a single mineral and a mineral mixture. The andesine series (a) is modified from the work of *Ramsey and Christensen* [1998]. The spectral range was limited to a low of 400 cm^{-1} in that work. In Figure 7b, a series of spectra from a Deccan Traps flood basalt sample in solid to powdered form is shown, courtesy of V. E. Hamilton. All spectra are shown with 2 cm^{-1} sampling.

with each other and to laboratory spectra of coarse- and fine-particulate samples. Laboratory spectra from basaltic materials are well-suited to such a comparison. The work of *Christensen et al.* [2000a] and *Bandfield et al.* [2000a] demonstrates that the spectrum of a Deccan Traps flood basalt sample (primarily plagioclase and clinopyroxene [*Hamilton and Christensen*, 2000]) in coarse-particulate form matches well with atmospherically corrected spectra of some dark regions (e.g., Cimmeria Terra and Syrtis Major). The Deccan spectrum thus serves as an example of the emissivity behavior of coarse-particulate material from some dark regions on Mars. Without a generally

recognized mineralogy for bright dust, it is useful to start with the assumption that the dust is dominated by silicate minerals. The Viking lander and Pathfinder measurements of soil chemistry clearly support this assumption [e.g., *Morris et al.*, 2000]. It has been shown recently that the soil precursor material may be basaltic in composition [*McSween and Keil*, 2000; *Morris et al.*, 2000]. Therefore a spectrum of the Deccan sample in fine-particulate form serves as a starting point for examining bright-region spectra. For the sake of the current analysis, little is changed if clays or palagonites are included. Figure 8 shows the spectra of Arabia and Syrtis Major from Figure 5a as
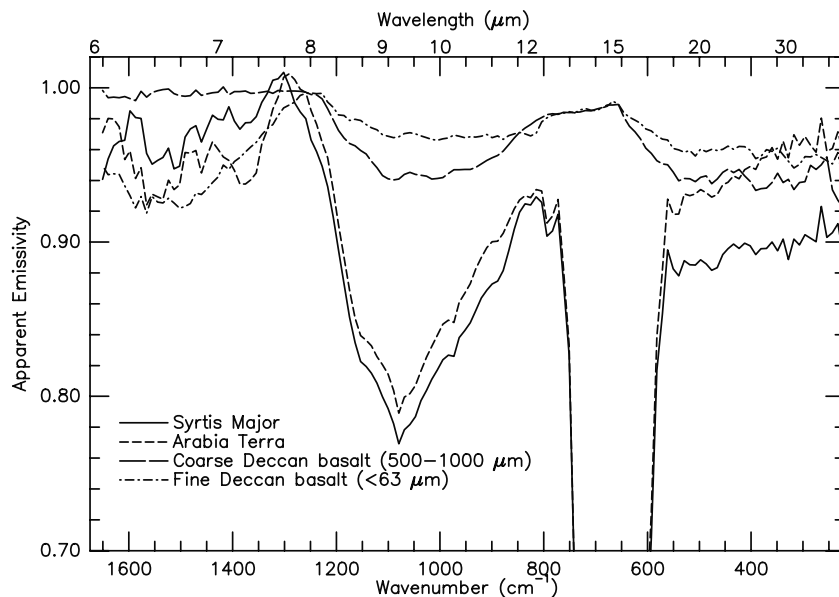
Figure 8. A comparison of laboratory spectra from coarse- and fine-particulate Deccan Traps basalt with TES spectra of a bright and dark region on Mars. Evidence for particle size effects in the spectra of Martian bright regions is suggested from this comparison.

representatives of typical bright and dark regions, respectively. Also shown are the spectra of Deccan basalt in coarse (710–1000 μm) and fine-particulate form (<63 μm). From this figure and further analysis of Figure 5, it is possible to see the evidence of particle size effects in TES spectra.

[25] At low wavenumbers (<560 cm^{-1}), bright-region TES spectra have higher emissivity than dark-region spectra (Figure 8 and Figures 5a and 5b). This characteristic is consistent with the reduced spectral contrast (higher emissivity) observed for the fine-particulate Deccan basalt relative to the coarse form. Atmospheric dust dominates the middle range (1300–780 cm^{-1}) of TES spectra making it difficult to assess the difference in surface emissivity of spectra from different orbits. However, there is clear indication in the spectra of adjacent bright and dark surfaces from the same orbit that bright surfaces typically have higher emissivity than dark surfaces (e.g., Figure 3). This behavior is also evident for TES spectra from cloudy atmospheric periods when dust is minimized (Figure 5b). The higher emissivity shown by bright regions in the middle spectral range is consistent with the reduced spectral contrast observed for the fine-particulate Deccan basalt.

[26] In the >1300 cm^{-1} range, atmospheric absorptions due to water vapor and CO_2 account for most of the detailed spectral structure. However, bright regions have significantly lower overall emissivity in this range compared with dark regions, suggestive of the high wavenumber transparency feature observed in the fine-particulate Deccan basalt.

[27] Although the spectral differences between bright and dark regions are consistent with those shown by Deccan basalt in fine and coarse form, all silicates produce spectral particle size effects that are similar to the observed bright/dark region differences. Figure 9 shows laboratory emissivity spectra from the ASU spectral library [*Christensen et al.*, 2000c] and hemispherical reflectance spectra from the JPL ASTER library converted to emissivity for three classes of minerals that are possible components of Martian dust.

When compared with carbonates and sulfates, the particle size effects of silicates (Figures 9a–9c) are most consistent with the TES observations. Fine-particulate carbonates produce a dramatic set of transparency features in the range <1300 cm^{-1} compared with their coarse form (Figures 9d–9f) that does not match the observed bright/dark spectral differences. Fine-particulate sulfates (Figures 9g–9i) show a strong, high wavenumber transparency feature like silicates but their behavior in the range <∼1300 cm^{-1} is more variable

4.3. Compositional Details

[28] Sections 4.3.1 and 4.3.2 describe two approaches to extract details from the spectra of bright regions that can serve to refine the mineralogy of surface dust.

4.3.1. High Wavenumber Transparency Feature

[29] Laboratory spectra of fine-particulate silicate minerals and rocks display variations in the high wavenumber transparency feature (>∼1100 cm^{-1}) that are a function of composition [*Salisbury et al.*, 1987, 1991; *Salisbury and Walter*, 1989]. As an example of these variations, Figure 10 shows spectra of three candidate materials for Martian surface dust. Because the high wavenumber transparency feature typically is the most intense absorption in the spectrum of fine-particulate silicates and contains composition-related details, it is potentially useful for analyzing the mineralogy of Martian surface dust.

[30] TES spectra in the range >1300 cm^{-1} contain absorptions due to atmospheric water vapor and CO_2 (Figure 2) in addition to the apparent transparency feature described previously. Because water vapor is a trace gas in the Martian atmosphere, it produces only minor absorptions that can be modeled readily. The CO_2 absorption centered at ∼1365 cm^{-1} is due to a stretching mode of the isotopic molecule $^{16}O^{12}C^{18}O$. This absorption is not a hot band so its intensity is independent of the absolute temperature of the atmosphere, making it easier to model. The
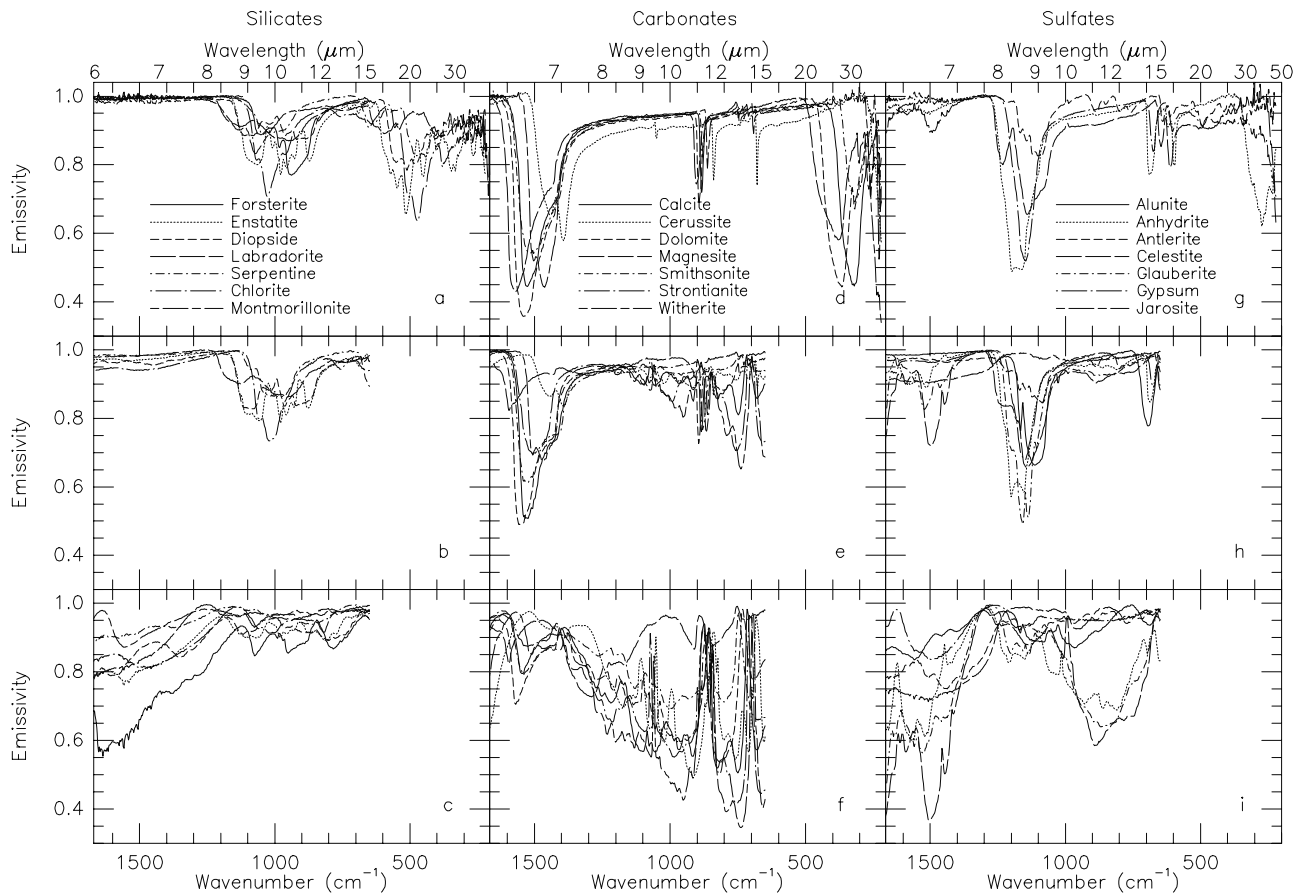
Figure 9. Emissivity spectra of particle size suites for three classes of minerals that may be present in Martian surface dust. The top row contains spectra from the ASU spectral library in the size range of 710–1000 μm for the silicates and sulfates and hand sample specimens for the carbonates. The middle and bottom rows contain spectra reproduced from the ASTER Spectral Library through the courtesy of the Jet Propulsion Laboratory, California Institute of Technology, Pasadena, California. Copyright © 1999, California Institute of Technology. ALL RIGHTS RESERVED. The ASTER library spectra were measured in hemispherical reflection mode and converted to emissivity using $E = 1 - R$. These spectra do not include the range $<\sim700$ cm^{-1}. The middle row covers the particle size range of 125–500 μm and the bottom row is 0–45 μm. In all cases attention was given to matching samples from the ASU library with those from the ASTER library based on chemical and spectral similarities. The ASU library lacked the carbonate strontianite and the sulfates alunite, glauberite, and jarosite.

spectral contribution of atmospheric dust in the range >1300 cm^{-1} has not yet been modeled for TES spectra. However, a qualitative assessment is possible by examining this spectral region under varying dust-load conditions (Figure 11). It is apparent from Figure 11 that atmospheric dust does not produce significant absorptions at high wavenumbers. Water-ice clouds have an effect in this spectral region, especially when combined with increased water vapor as evidenced by the differences between the dusty and cloudy spectra in Figure 5c. However, many TES spectra are available that are effectively free of cloud absorptions.

[31] The spectra of Arabia and Syrtis from Figure 5a have minimal water-ice cloud absorptions and are representative of the high wavenumber spectral behavior of bright and dark regions. Figure 12 shows these spectra along with a modeled spectrum (J. Pearl and G. Bjoraker, personal communication) of combined water vapor and CO$_2$ produced using the following generic conditions: 10 precipitable microns (pr μm) of water vapor, an atmospheric temperature profile starting at 260 K at the surface and following a standard lapse rate, and a surface temperature of 300 K. Much of the detailed structure of the TES spectra in the range >1300 cm^{-1} is matched by the modeled spectrum, especially for the Syrtis spectrum. Dividing the modeled atmosphere spectrum from the Martian spectra produces a partial atmospheric correction, allowing a more accurate look at surface emissivity in the high wavenumber range (Figure 12b). Although many remaining sharp features indicate an incomplete removal of water vapor, it is significant that the well-resolved spectral feature centered at ~1365 cm^{-1} in the bright-region spectrum in Figure 12a is nearly absent. This result casts doubt on the sulfate interpretation for this feature by *Clark and Hoefen* [2000]. An analysis by *McAfee and Kirkland* [2000] described the potential for just such a
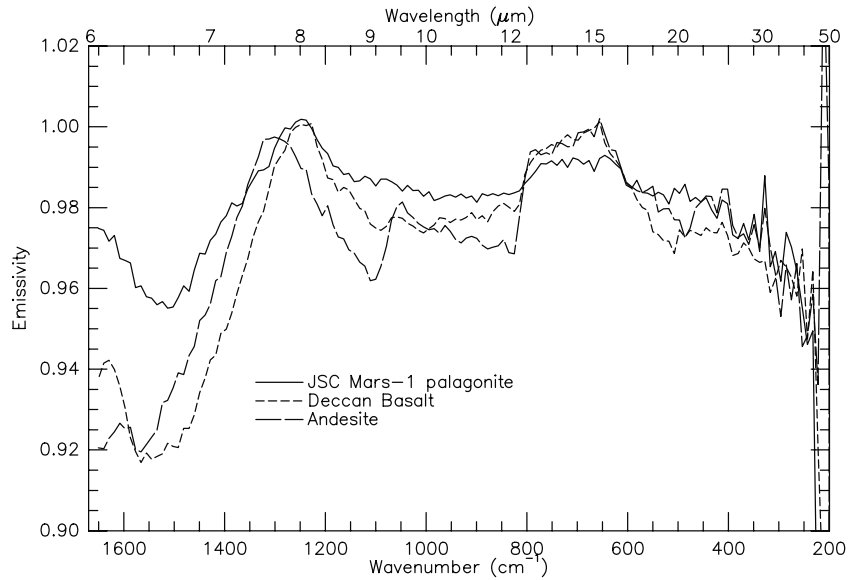
Figure 10. Candidate materials for Martian surface dust. These spectra were measured from samples ground and sieved to a size <63 μm; they are shown at the TES spectral resolution of 10 cm^{-1}. Unlike the coarse particulate form of these materials, the fine particulates display spectral information at high wavenumbers (>1200 cm^{-1}) that is related to composition. Basalt and andesite spectra are courtesy of V. E. Hamilton. For a description of JSC Mars-1, see work by *Allen et al.* [1998].

misinterpretation. Further refinement of the mineralogical information present in the high wavenumber transparency feature will be possible using more accurate atmospheric modeling than presented here and a library of spectra from fine-particulate materials.

4.3.2. Spectral Ratios

[32] A ratio of spectra from two different locations can serve to cancel atmospheric contributions and reveal surface emissivity [e.g., *Pollack et al.*, 1990; *Moersch et al.*, 1997;

Hoefen et al., 2000] but it requires certain assumptions and applies only to restricted conditions. Any ratio spectrum represents a combination of spectral features of the two surfaces from which the spectra were measured. If the spectral character of one of the two surfaces is reasonably well constrained, the spectral features of the other surface can be investigated. To fully evaluate the caveats and assumptions inherent in spectral ratio analysis, the equation presented by *Smith et al.* [2000b] that describes observed
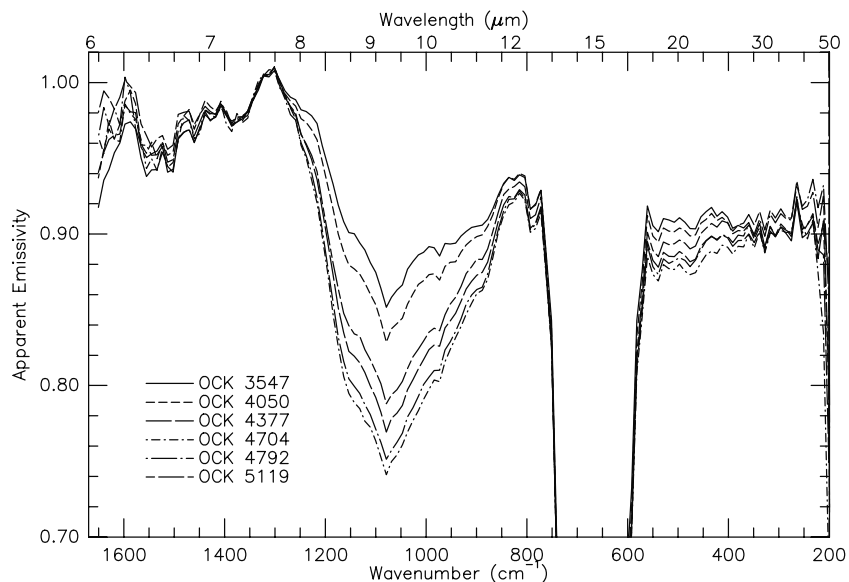
Figure 11. A qualitative assessment of the contribution of atmospheric dust to TES spectra in the range >1300 cm^{-1}. Six different spectra (averages using ICK 1835:1854 from the OCK shown) from a common location in Syrtis Major show varying amounts of atmospheric dust. Little change is evident at high wavenumbers (>1300 cm^{-1}) in spite of the significant changes over the rest of the spectral range. This suggests that the contribution of atmospheric dust at high wavenumbers is small.
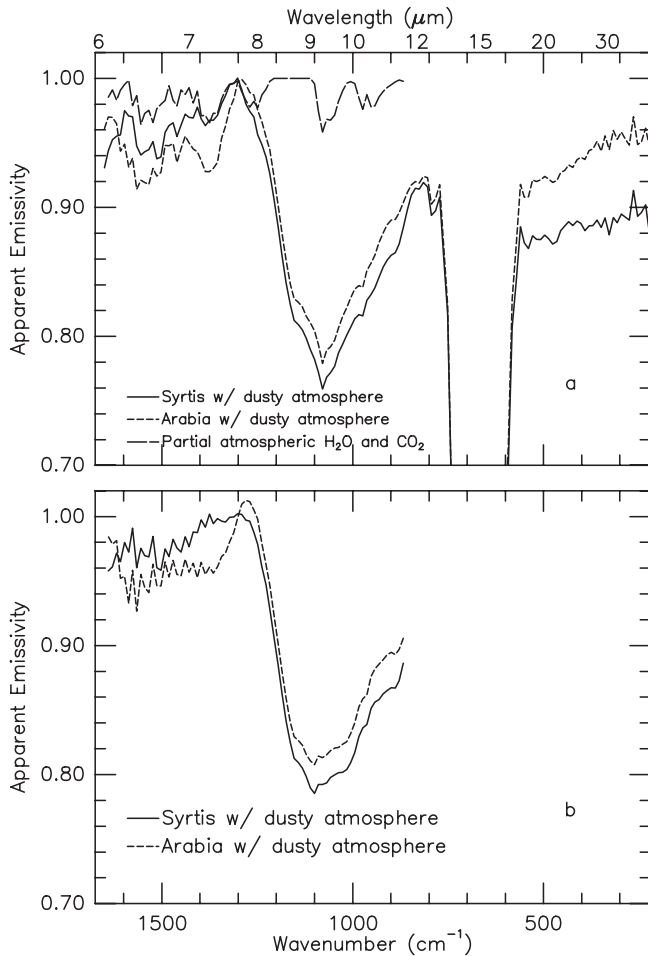
Figure 12. Analysis of the contribution of atmospheric water vapor and CO_2 to the spectral character at the high wavenumber end of TES spectra. In Figure 11a, a partial spectrum of H_2O and CO_2 modeled from generic atmospheric conditions (see text) is shown in comparison to averaged spectra from a dark region (Syrtis Major) and a bright region (Arabia). By dividing out the atmosphere spectrum, it is possible to see the residual spectral character of the surface (Figure 11b). Bright regions typically show greater spectral contrast at high wavenumbers than dark regions.

radiance as a function of wavenumber $I_{obs}(\tilde{v})$ measured from orbit is reproduced here.

$$I_{obs}(\tilde{v}) = \varepsilon(\tilde{v})B[T_{surf}, \tilde{v}]e^{-\tau_0(\tilde{v})/\mu} + \int_0^{\tau_0} B[T(\tau), \tilde{v}]e^{-\tau(\tilde{v})/\mu}d\tau \quad (1)$$

The quantity $\varepsilon(\tilde{v})$ is surface emissivity as a function of wavenumber, $B[T_{surf}, \tilde{v}]$ is the Planck function at surface temperature $T_{surf}(K)$, $\tau_0(\tilde{v})$ is the normal column-integrated aerosol opacity, μ is the cosine of the emission angle, $T(\tau)$ is the atmospheric temperature profile, and the integral is calculated over the range of $\tau = 0$ at the spacecraft to τ_0 at the surface. The first term of the equation (1) describes the attenuation by the atmosphere of radiation emitted by The surface. The second term represents the upwelling

emission of the atmosphere. Incident solar radiation reflected back to the spacecraft and scattering by atmospheric aerosols are neglected in this equation because of their small contribution.

[33] In a ratio of two emissivity spectra, the Planck quantity of the surface component already is removed, thus eliminating one of the variables in equation (1). For conditions where atmospheric opacity is low (≤ 0.25) [*Smith et al.*, 2000b] and surface temperature is greater than atmospheric temperature, upwelling emission of the atmosphere is assumed to be negligible. These conditions are typical for daytime TES measurements away from dust storm activity. In this case, a ratio will cancel the spectral contribution of the atmosphere assuming the conditions of the atmosphere are the same for the two locations from which the spectra are measured. This situation is best ensured using locations that are close to each other both in lateral distance and elevation and only applies to spectra from the same orbit and with the same emission angle. Because water-ice clouds are variable over small spatial scales, spectra measured during cloudy conditions should not be used in a ratio intended for surface analysis. An example and interpretation of a spectral ratio with implications for dust mineralogy is given in section 6.

5. A Dust Cover Index Based on Particle Size Effects

5.1. Index Definition

[34] The apparent particle size effects observed in TES spectra of bright regions serve as an indicator for the presence of fine particles or dust on the surface. Beginning with the assumption that bright-region dust is dominated by silicates, the spectral range best suited to identifying particle size effects and hence the presence of dust is $> \sim 1300$ cm^{-1}. This is a range where k is very low and n is close to unity, producing a broad, deep transparency feature in fine-particulate silicates (Figure 9c). For TES spectra, Figure 5c shows that the $1350 - 1400$ cm^{-1} range retains a significant emissivity separation between bright and dark regions regardless of atmospheric conditions. Although an isotopic CO_2 gas absorption occurs here, its intensity is relatively invariant as long as surface temperature is greater than that of the atmosphere, a condition typical for daytime TES observations away from dust storms. This is shown in Figure 13 where a series of synthetic Martian atmospheric spectra for CO_2 and water vapor have been generated for various temperature conditions. For the cases where the surface is warmer than the atmosphere, the maximum variation in emissivity of the CO_2 absorption centered at 1367 cm^{-1} is 0.005. In contrast, the minimum delta emissivity between the bright and dark region spectra of Figure 5c is 0.018 at this wavenumber. Therefore variations in the depth of the CO_2 feature cannot account for the difference in emissivity of these bright and dark region spectra. Instead, the variation must be attributable to surface emissivity. For silicate materials, variation in particle size is the most likely contributor to the variation in emissivity in the spectral range $> \sim 1300$ cm^{-1}. Absorptions due to atmospheric water vapor are not significant at wavenumbers $< \sim 1400$. We therefore define a dust cover index (DCI) to be equal to the average emissivity value from 1350 to 1400 cm^{-1}. This spectral region is least affected by atmospheric components
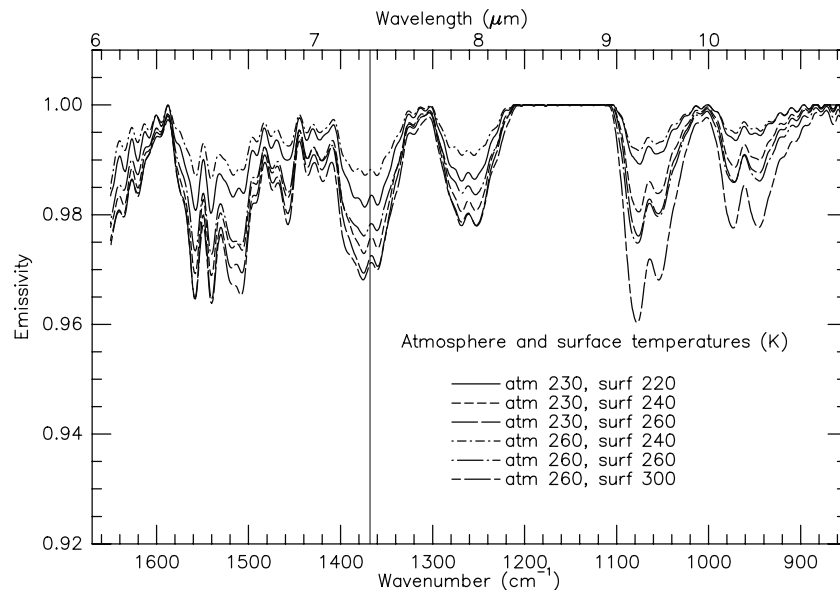
Figure 13. Variations in band depth of atmospheric water vapor and CO_2 with changes in surface and atmospheric temperatures. These spectra were modeled using water vapor at a mixing ratio of 137 ppm up to the condensation level, surface pressure of 6.1 mbars, and surface temperatures as shown. Atmospheric temperatures shown indicate the temperature at the 6.1 mbar level with a lapse rate of -3 K km^{-1} up to 30 km. The CO_2 isotope band centered at $\sim$1365 cm^{-1} (vertical line) is in the region chosen for the DCI. However, its depth does not change significantly when the surface is warmer than the atmosphere (bottom three spectra), which is typical for afternoon, nondust-storm conditions on Mars. Therefore any significant variations in emissivity in this spectral location likely are due to surface emissivity.

yet is sensitive to the spectral particle size effects of silicates. A statistical analysis of this index relative to the global data set is given in the next section.

5.2. Global Dust Cover Map

[35] A global map of the DCI is presented in Figure 14. This map was produced using TES mapping-orbit, nadir-pointing, daytime data constrained using the following quality fields: QUALITY:MAJOR_PHASE_INVERSION 0 0, QUALITY:ALGOR_RISK 0 0, QUALITY:HGA_MO-TION 1 1, and QUALITY:PNL_MOTION 1 1. In order to maximize the SNR, the data used for the map span a range of L_s that includes a summer season in both hemispheres ($103.6°-287.7°$) and incorporate only spectra with brightness temperatures $\geq$260 K. The temperature constraint had the effect of excluding the highest latitudes where surface temperatures did not meet the 260 K limit. The data were binned at eight pixels per degree and any gaps were filled using a linear interpolation between neighboring bins weighted by distance.

[36] The map shows a remarkable spatial coherence that clearly is related to Martian albedo features at many scales. A scatter plot of albedo and DCI values (Figure 15) has a linear correlation coefficient of -0.85, quantifying the extent of the correlation evident from the map. Also, apparent from the map is the spatial coherence of inter-mediate index values where concentric patterns of color appear in many places. No obvious artifacts due to atmospheric effects are evident. Although water-ice clouds are known to form in an equatorial belt during part of the year

[Pearl et al., 2001], there is no evidence for them in the global map. It is likely that binning of pixels from different orbits representing various atmospheric conditions has averaged out the cloud effect.

[37] Using maps of TES albedo and thermal inertia data binned at the same resolution (Figure 16), it is possible to quantify the extent to which DCI values relate to the presence or absence of surface dust. Thermal inertia data can be used to identify surfaces that are completely covered by dust. It is widely accepted that the lowest thermal inertia regions on the planet must be mantled with dust at least a few centimeters thick. New photogeological evidence for this view has been provided by the observation of dust avalanche scars in bright, low thermal inertia regions [Sullivan et al., 2001]. Based on the laboratory studies of Presley and Christensen [1997], surfaces with a thermal inertia value of 100 Jm^{-2}s$^{1/2}$K (hereafter abbreviated IU for inertia units) have particles with diameters of 6 μm or less. Therefore it can be expected that regions on Mars with a thermal inertia value of 100 IU or less will be covered by fine particulates that display spectral particle size effects. Dust-free surfaces are best identified by very low albedo values. Thermal inertia data are not well-suited to this task because, except for the extremely high values associated with bedrock, intermediate values have a non-unique interpretation and may result from mixtures of dust and coarse particles. Low albedo values however, likely are only possible in the absence of any significant dust accumulation. Low albedo regions like Syrtis Major have been observed to brighten following dust storms and then
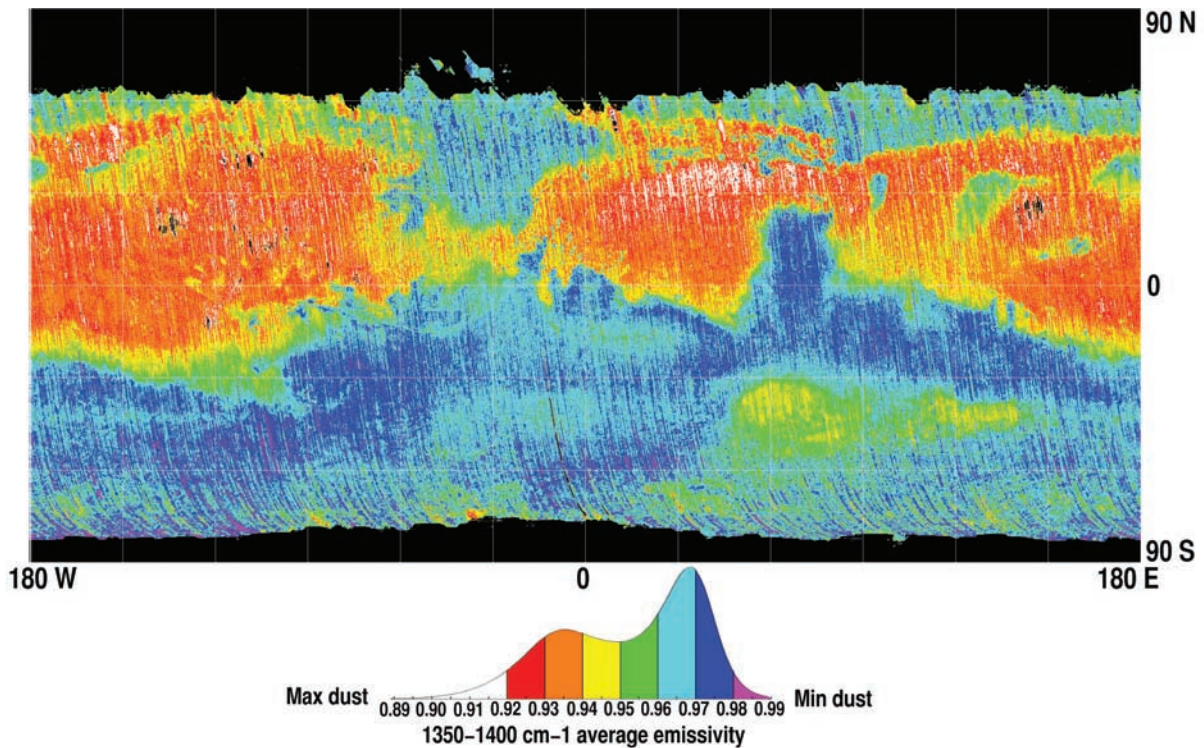
Figure 14. Map of the global DCI developed in this work. The average emissivity value in the 1350–1400 cm^{-1} range is shown, binned at eight pixels per degree with gaps filled by interpolation. The index is sensitive to the occurrence of silicate spectral particle size effects and thus serves as an indicator for the presence of silicate dust on the surface. Orange, red, and white colors indicate areas that likely are dust covered while blue and magenta areas likely are dust-free. The color scale bar is a histogram of the index values.

darken again over time indicating a process that is actively removing dust particles [*Christensen*, 1988]. Much of Syrtis and Acidalia as well, have albedo values ≤0.10 as measured by TES. This range of low albedo values serves as a proxy for dust-free or minimally dust-covered surfaces.

[38] Two histograms of the DCI are shown in Figure 17 that were compiled from the global data set for regions on the planet where thermal inertia is ≤100 IU and albedo is ≤0.10 representing dust-covered and dust-free surfaces, respectively. The average DCI value for dust-covered surfaces is 0.931 with a standard deviation of 0.009. Dust-free surfaces have an average value of 0.969 with a standard deviation of 0.007. The two histograms are well separated out to 2σ values (0.949 for dust-covered versus 0.955 for dust free), demonstrating the unique spectral character of the two Martian surface types in the range of the DCI.

6. Discussion

### 6.1. Interpretation of DCI Values

[39] The histogram included with the global DCI map (Figure 14) shows a bimodal distribution of the DCI values. Peaks at ∼0.935 and ∼0.97 correspond closely to the values indicative of dust-covered and dust-free surfaces, respectively, as described in section 5. The occurrence of a range of intermediate DCI values that appear spatially transitional

on the global map suggests that they may represent surfaces that are only partially obscured by dust. An alternative explanation is that intermediate DCI values represent indurated surfaces. In this view, fine particles are cemented to produce a crusted surface [e.g., *Jakosky and Christensen*, 1986]. Although the thermal IR spectral behavior of such material is not known, it is likely that a population of loose
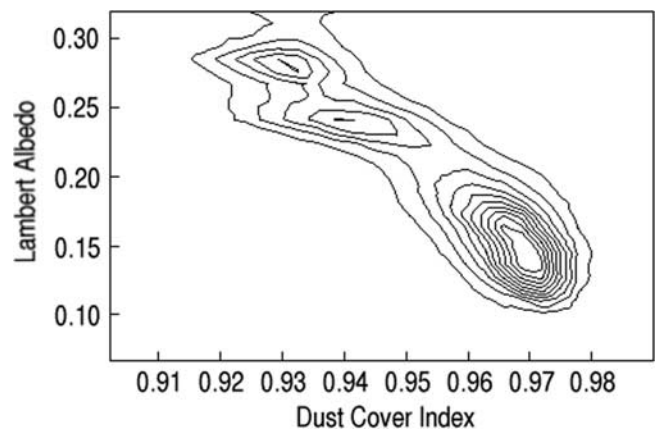
Figure 15. Scatter plot showing the relationship of the DCI (1350–1400 cm^{-1} average emissivity) to lambert albedo (0.3–3.0 μm). The linear correlation coefficient is −0.85.
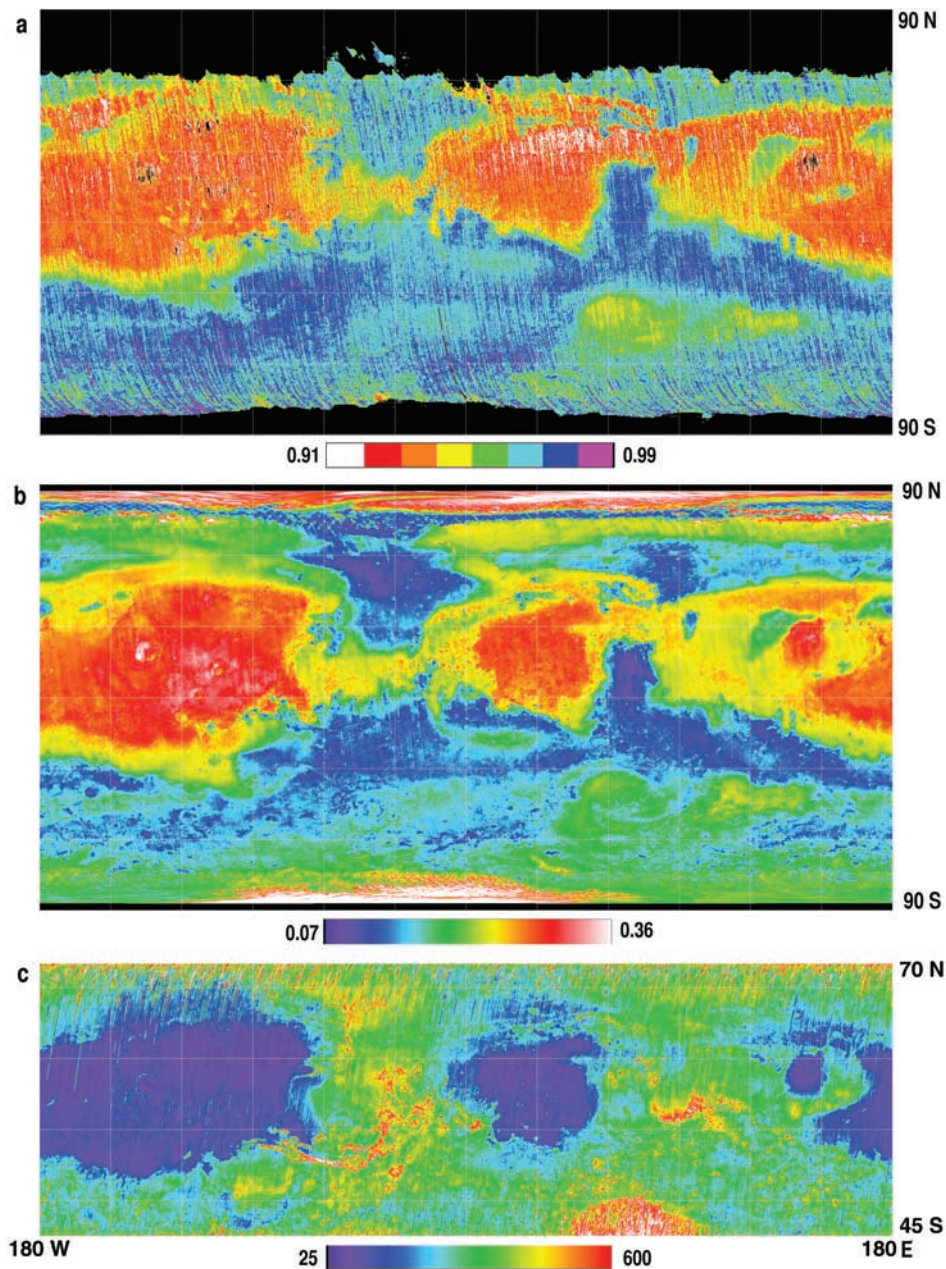
Figure 16. Comparison of the DCI with lambert albedo and thermal inertia. The color scale for the DCI map (a) and albedo (b) has been designed to emphasize the correlation between the two quantities. The thermal inertia values (Figure 16c) are in units of $Jm^{-2}s^{-1/2}K^{-1}$. Each quantity is sensitive to a different skin-depth, supplying complementary but not always the same information concerning the uppermost surface layer of Mars.

fines would still be present and could contribute measurable particle size effects to the spectrum. These fines could lower the 1350–1400 cm^{-1} emissivity average enough to produce an intermediate DCI value.

[40] Classification threshold values for dust-covered and dust-free surfaces can be established using the histograms of Figure 17. The lack of overlap of the 2σ values observed for the two histograms suggests possible thresholds at 0.949 for dust-covered and 0.955 for dust-free surfaces. However, these values provide only a narrow intermediate range for the likely cases where surfaces display a range of dust

cover. Therefore the more conservative 1σ values of 0.940 and 0.962 will be used to represent dust-covered and dust-free surfaces, respectively, and those values that are intermediate probably represent surfaces that are partially dust covered.

6.2. Applications of the DCI

[41] Albedo, thermal inertia, and the DCI all can be used to characterize the uppermost layer of the Martian surface. Albedo and thermal inertia measurements have skin-depths on the order of a few microns and a few to several
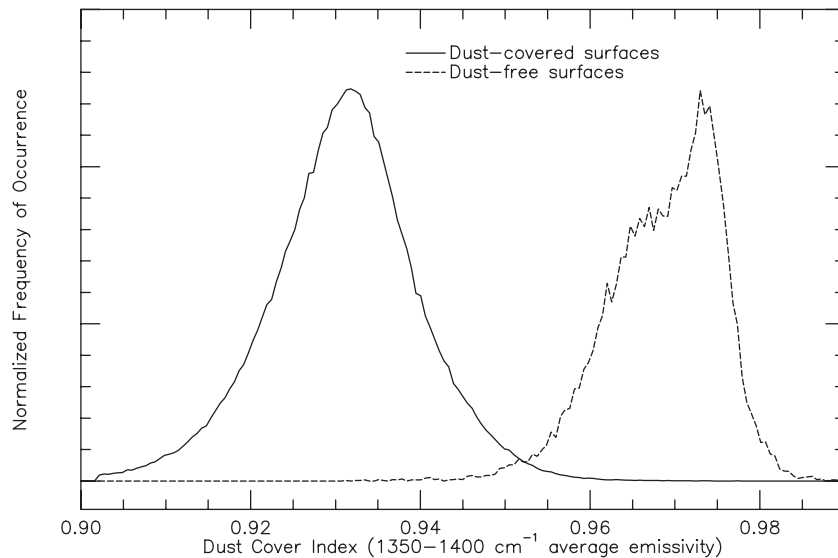
Figure 17. Histograms of the DCI for dust-covered and dust-free surfaces. Dust-covered surfaces were identified as locations on the planet that have a thermal inertia ≤ 100 Jm^{-2}s$^{1/2}$K. At a spatial resolution of eight TES pixels per degree, 435,778 values were used in this histogram. Dust-free surfaces were identified as locations with an albedo ≤ 0.10. A total of 52,163 values were used for this histogram and then normalized to match the height of the histogram for dust-covered surfaces. The DCI spectral parameter clearly distinguishes the two surface types.

centimeters, respectively, while the DCI is sensitive to accumulations whose thickness is on the order of the penetration depth of thermal-IR wavelengths, which is a few tens of microns. Figure 16 combines maps of DCI, albedo, and thermal inertia values to facilitate comparisons of the three data sets. The color scheme used to produce the DCI map (Figure 16a) was chosen to mimic that of albedo (Figure 16b) in order to enhance intercomparison of the two parameters. The three maps are grossly similar, especially the DCI and albedo maps. However, there are places where the albedo and thermal inertia maps are more comparable to each other than to the DCI map. For example, the shape of the highest albedo region in Arabia (orange to red colors in Figure 16b) is well matched by the lowest thermal inertia values in Arabia (blue to magenta colors in Figure 16c). A similar spatial pattern for the DCI is not present, especially in northeastern Arabia (Figure 16a). In fact, DCI values do not vary significantly from northeastern Arabia, across the top of Syrtis, and into western Utopia Planitia while albedo and thermal inertia values do vary. One interpretation for this observation is that there exists a mantle of dust in the region that is thick enough and continuous enough to produce strong spectral particle size effects but without fully obscuring, in a thermal inertia sense, the underlying materials. Such a layer could be on the order of a several tens of microns to a few millimeters thick, a thickness less than the skin-depth of thermal inertia measurements but thick enough to produce the observed spectral behavior [*Crisp and Bartholomew*, 1992; *Johnson et al.*, 2002]. The subtle change in albedo across the region may be due to a transition from a thick mantle of dust in central Arabia to a much thinner but still continuous layer in western Utopia. Much of eastern Elysium displays a similar set of albedo, thermal inertia, and DCI values possibly indicating similar surface conditions.

[42] At a local scale, the DCI can be used to investigate the surface character of the ''White Rock'' feature in Pollack Crater (8°S, 25°E). *Ruff et al.* [2001] presented thermal inertia and geomorphic evidence that White Rock is not covered by a mantle of dust. The DCI value also supports this conclusion. Using the average spectrum of White Rock material from that work, the DCI value is 0.962, which is right at the threshold for dust-free surfaces. There are other similar intracrater deposits in western Arabia that can be examined in this way to establish whether they represent relatively high albedo material that is not simply a dust mantle.

[43] The DCI also is useful for investigating the physical character of dark surfaces. Although the general paradigm is that low albedo regions have surfaces composed of relatively coarse, dust-free materials, some evidence has been presented that dark dust may also exist on Mars. Using Mars 5 photopolarimetry data, *Dollfus et al.* [1993] suggested that dark dust is present as a strongly bound coating on coarser, surface particulates in Mare Erythraeum south of Valles Marineris. The average DCI value for this region is 0.970 which is inconsistent with the presence of loose dust. However, it is unclear whether the strongly adhering coating of dust suggested by Dollfus et al. would still produce spectral particle size effects, so some ambiguity remains. The particle size of the material forming dark wind streaks in western Arabia/Oxia Palus recently has been revisited by *Edgett and Malin* [2000] who suggested that they are deposits of dark silt rather than sand. This suggestion can be investigated using the DCI. Inspection of the DCI map from this region (Figure 18) reveals that the streaks have index values that are too high (≥ 0.96) to indicate a significant abundance of particles <100 μm in size. Although neither of these analyses rules out the possibility of a population of low albedo fines on the planet, no low
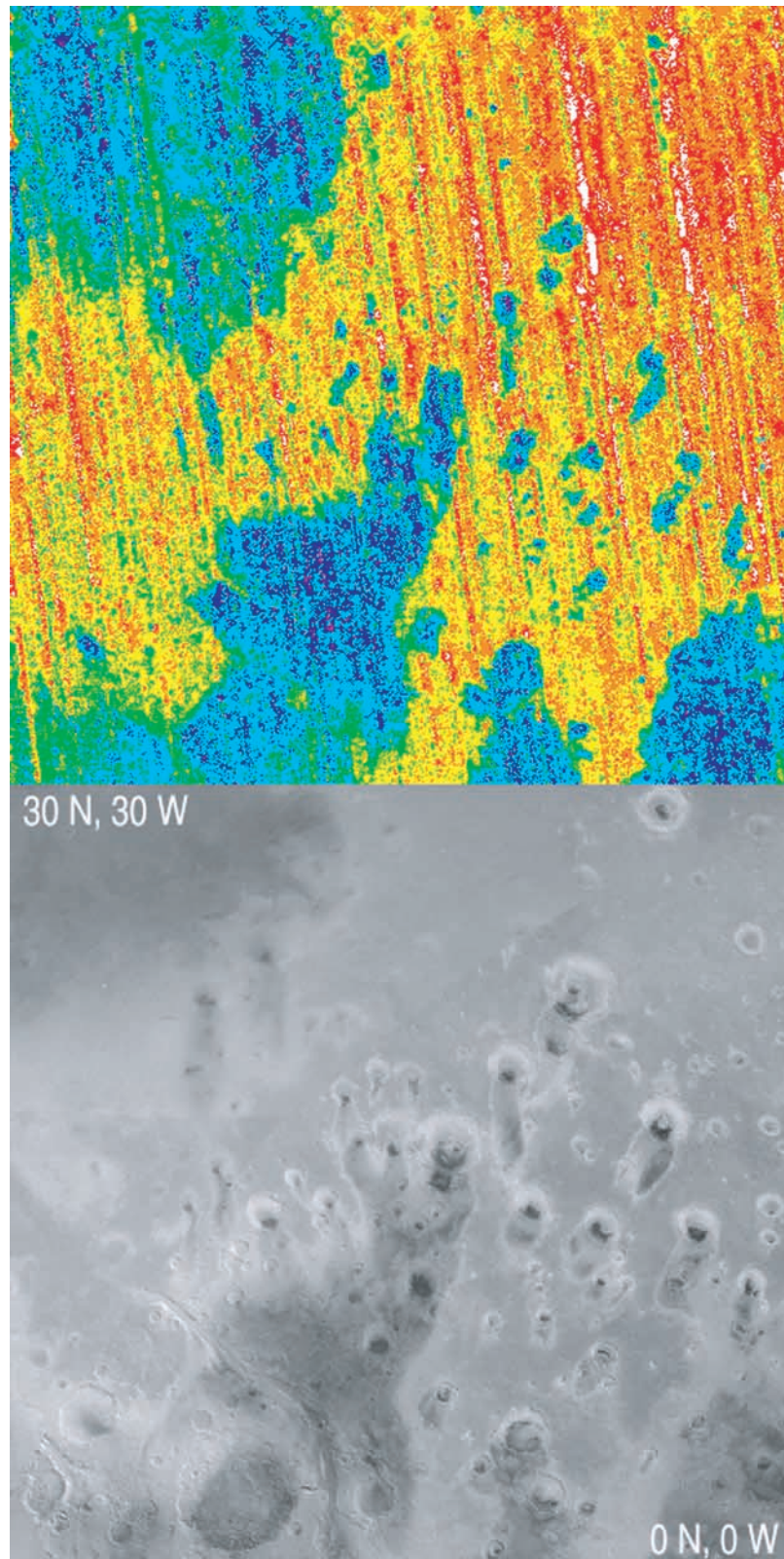
Figure 18.   Analysis of crater dark streaks in western Arabia/Oxia Palus. The upper frame displays the DCI values using the same color scale as in Figure 5. The lower frame is a mosaic of Viking Orbiter images. Dark streaks show up in blue, indicating that they are not composed of fine-particulate silicates, i.e., they are dominated by particles >100 μm in size.
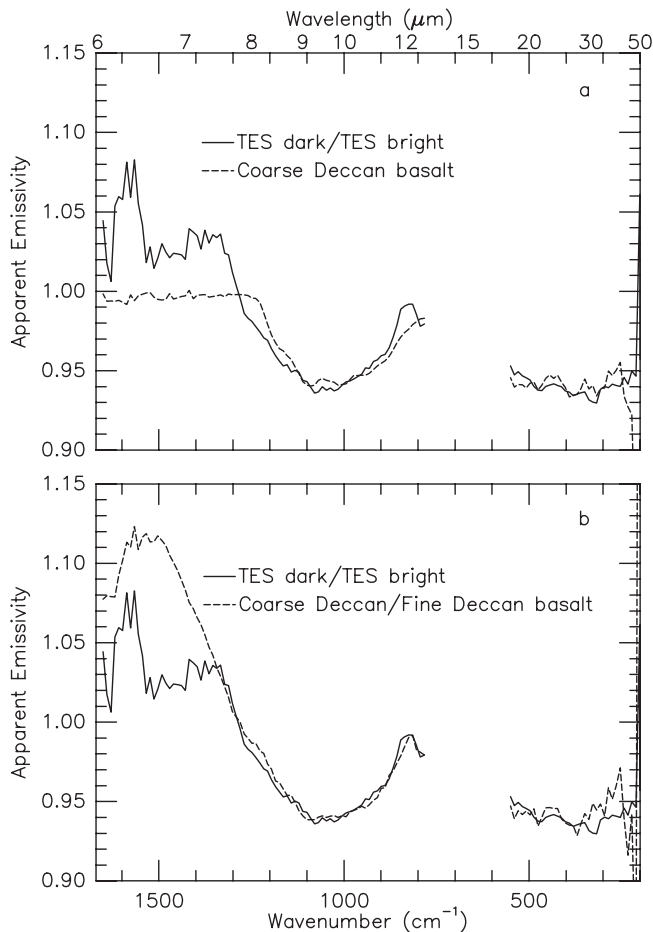
Figure 19. Spectral ratio analysis of bright and dark surfaces. (a) A ratio of the TES spectra from the dark splotch and bright floor of the crater shown in Figure 3. A laboratory spectrum of Deccan basalt is shown for comparison. (b) The same ratio of TES spectra from (a) compared with a ratio of laboratory spectra of coarse (500–1000 μm) and fine (<63 μm) particulate Deccan basalt. The quality of the match to the TES spectral ratio is much better than with the coarse Deccan basalt by itself, suggesting that the bright-surface material has nonunit emissivity with spectral characteristics similar to fine Deccan basalt.

albedo surfaces have yet been found that display the spectral effects of fine silicate particles.

### 6.3. Dust Mineralogy Based on Spectral Ratio Analysis

[44] Dark intracrater splotches on the floor of bright craters are well-suited to the investigation of surface spectral character using a ratio, a strategy described by *Ruff and Christensen* [1999] and used by *Johnson et al.* [2002]. Atmospheric variations are minimized due to the close proximity, both in distance and elevation, of the bright and dark surfaces. In many cases these surfaces are large enough that spectra from several TES pixels can be averaged together for improved SNR. The intracrater splotch presented in Figure 3a is used as an example, with the spectra from Figure 3b used to produce a ratio of a dark to bright surface. The result is shown in Figure 19a. A spectrum of coarse-particulate Deccan flood basalt, which

represents a good candidate spectrum for comparison, is included in this figure. The prominent V-shape of atmospheric dust is notably absent in the ratio spectrum as are many of the sharp CO_2 and water vapor features, an indication of the quality of the atmospheric cancellation. The ratio spectrum is broadly similar to the Deccan basalt spectrum but there are significant differences. Most obvious is the mismatch in the region $>\sim1300$ cm^{-1} where the ratio spectrum rises above unity. Because emissivity >1.0 is not physically possible, it indicates a contribution from the
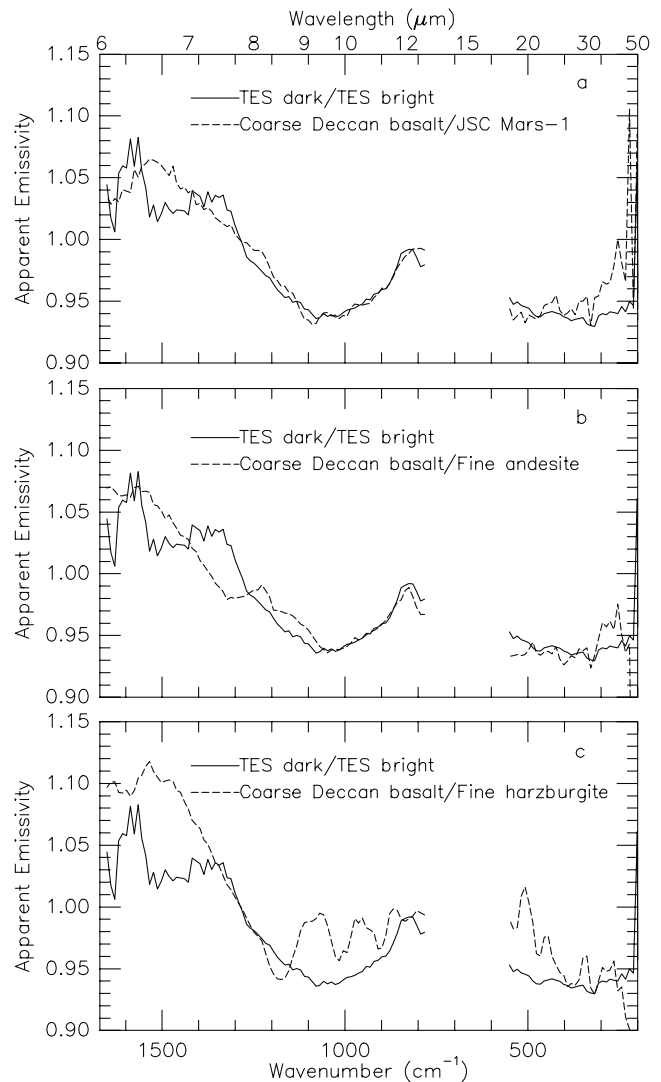
Figure 20. Comparison of the TES spectral ratio in Figure 19 to the following laboratory ratio-spectra: (a) coarse (500–1000 μm) Deccan basalt divided by fine (<63 μm) JSC Mars-1 palagonite; (b) coarse Deccan basalt divided by fine (<63 μm) andesite; and (c) coarse Deccan basalt divided by fine (<63 μm) harzburgite. None of these ratios matches as well as the coarse and fine Deccan basalt ratio of Figure 19b. Only the plagioclase-rich andesite produces a good match to the peak at ~825 cm^{-1} in the TES spectral ratio, an indication that fine-particulate plagioclase may be a component of the bright-surface material on the crater floor (see Figure 21).
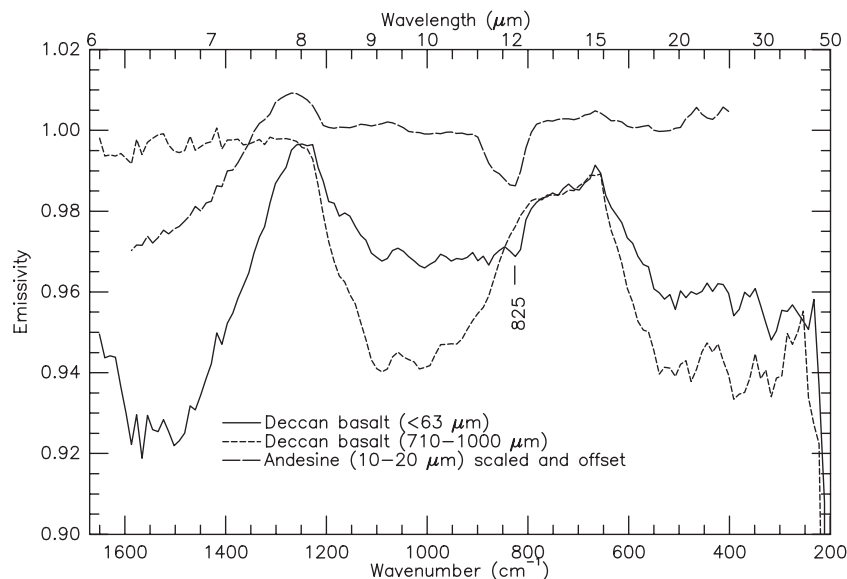
Figure 21. Evidence of a plagioclase-related transparency feature in the spectrum of fine (<63 μm) Deccan basalt. The feature at ~825 cm^{-1}, absent in the coarse Deccan basalt, is likely due to fine-particulate andesine (An$_{30-50}$). A feature at this location is evident in TES spectra from some Martian bright regions based on spectral ratio analysis (see Figure 19).

bright-surface spectrum in the denominator. A less obvious yet significant mismatch is the prominent peak centered at ~825 cm^{-1} that likely is a feature of the bright-surface spectrum, as shown below.

[45] Because a ratio spectrum contains the contributions from two different spectra, it is inappropriate to interpret it as a single spectrum. Instead, it can be compared to a spectrum that is itself a ratio of two spectra. If it is assumed that the dark surface is composed of coarse-particulate basaltic material like the Deccan basalt and the bright surface is the fine-particulate equivalent, then a ratio of the spectra of these candidate materials can be compared with the dark/bright spectral ratio. The result, shown in Figure 19b, is a remarkably good match between the spectral ratio of laboratory basalt samples and the Martian dark/bright ratio. The U-shape between ~1300 and 780 cm^{-1} is well matched, including the prominent peak at ~825 cm^{-1}. For the range >1300 cm^{-1}, the match is not as good, possibly due to incomplete cancellation of atmospheric water vapor features, but the increase in emissivity above unity is the correct trend for a ratio of coarse to fine particle sizes. Spectral ratio analysis produces similar results for many of the craters in western Arabia Terra that host dark materials.

[46] To test the uniqueness of the coarse and fine Deccan basalt result, three different candidate spectra of fine-particulate materials were substituted into the denominator of the ratio in place of the fine-particulate Deccan basalt spectrum (Figure 20). Substituting the spectrum of JSC Mars-1 palagonite [*Allen et al.*, 1998] of Figure 10 does not fully reproduce the broad, U-shape of the dark/bright ratio or the peak at ~825 cm^{-1}, but matches better the magnitude of the emissivity in the region >1300 cm^{-1} (Figure 20a). A ratio using the fine-particulate andesite spectrum [*Wyatt et al.*, 2001] of Figure 10 in the denominator provides a good match to the ~825 cm^{-1} peak but a poor match of the

broad, U-shape (Figure 20b). Substituting into the denominator a spectrum of fine-particulate material with a very mafic composition (harzburgite) [*Hamilton*, 1998] produces a very poor match to the dark/bright ratio (Figure 20c). Only the andesite and Deccan basalt spectra produce a good match to the peak at ~825 cm^{-1} in the dark/bright ratio spectrum. It is in this location that fine-particulate plagioclase minerals have a prominent transparency feature, as demonstrated by the andesine (An$_{48}$) spectra of Figure 7a. Both the andesite and Deccan basalt have a significant plagioclase component (53% [*Wyatt et al.*, 2001] and 65% [*Hamilton*, 1998], respectively). The JSC Mars-1 palagonite is assumed to have much less plagioclase based on considerations of its chemistry [*Allen et al.*, 1998] and parent material [*Morris et al.*, 1993] and the harzburgite has only 10% plagioclase [*Hamilton*, 1998]. The fine-particulate plagioclase transparency feature is evident in the spectrum of <63 μm Deccan basalt as shown in Figure 21. It is also apparent from this figure how the spectral ratio of coarse- and fine-particulate Deccan basalt produces a peak centered at ~825 cm^{-1}.

[47] Evidence of subtle spectral features in Martian surface dust also is emerging in the work of *Bandfield and Smith* [2001] where previously it was assumed that surface dust was spectrally featureless [*Christensen et al.*, 2000a; *Smith et al.*, 2000a]. A distinctive spectral feature at ~825 cm^{-1} appears in the spectra of large bright regions as a result of using multiple emission angle observations to improve the surface-atmosphere separation (J. Bandfield, personal communication). This new observation thus supports evidence from dark/bright ratio spectra that there exists a feature at ~825 cm^{-1} in bright surface dust. Bandfield also has attributed this feature to plagioclase in fine-particulate form. In an analysis of lunar soil spectra by *Salisbury et al.* [1997], a similar conclusion was reached for the interpretation of a prominent trans-

parency feature found in a similar location in many of the samples.

7. Conclusions

[48] Direct comparison of thermal-IR spectra from bright and dark regions on Mars leads to the following conclusions.

1. Spectral information attributable to surface emissivity is apparent without performing a surface-atmosphere separation.

2. The following spectral differences are typical of the behavior of the large, classical bright and dark regions on Mars as well as some smaller scale examples: Bright regions show reduced spectral contrast (increased emissivity) in the range $<\sim1300$ cm^{-1} and increased spectral contrast (decreased emissivity) in the range $>\sim1300$ cm^{-1} when compared with dark regions.

3. The spectral differences between bright and dark regions can be attributed to variations in the particle size of surface silicate materials.

4. The decrease in emissivity observed in the spectral range $>\sim1300$ cm^{-1} for bright regions likely is due to a transparency feature found in silicate materials whose particle size is <100 μm. This apparent transparency feature can be exploited to map the presence or absence of silicate dust on the Martian surface. The resulting dust cover index (DCI = $1350-1400$ cm^{-1} average emissivity) serves as a gauge of surface-obscuring dust that can impact spectral measurements and can be used to address questions about the physical character of the surface independently of thermal inertia and albedo.

5. Initial results show no evidence for dark silicate dust on Mars but do show that some bright regions (e.g., "White Rock") are relatively dust-free.

6. Spectral ratio analysis, when carefully applied, can be used as a means of surface-atmosphere separation to reveal details of the spectral characteristics of surface materials. Ratios of spectra from bright and dark surfaces that are in close proximity produce a spectral feature that can be interpreted as a transparency feature found in fine-particulate plagioclase feldspar or perhaps other minerals with similar crystallographic structure.

References

Adams, J. B., and T. B. McCord, Mars: Interpretation of spectral reflectivity of light and dark regions, *J. Geophys. Res.*, 74, 4851–4856, 1969.

Allen, C. C., K. M. Jager, R. V. Morris, D. J. Lindstrom, M. M. Lindstrom, and J. P. Lockwood, Martian soil simulant available for scientific, educational study, *Eos. Trans. AGU*, 79, 405–409, 1998.

Bandfield, J. L., and M. D. Smith, Multiple emission angle surface-atmosphere separations of MGS Thermal Emission Spectrometer data, in *Lunar Planet. Sci. XXXII*, abstract 1596 [CD-ROM], 2001.

Bandfield, J. L., V. E. Hamilton, and P. R. Christensen, A global view of Martian volcanic compositions from MGS-TES, *Science*, 287, 1626–1630, 2000a.

Bandfield, J. L., P. R. Christensen, and M. D. Smith, Spectral data set factor analysis and end-member recovery: Application to analysis of Martian atmospheric particulates, *J. Geophys. Res.*, 105, 9573–9587, 2000b.

Beish, J. D., and D. C. Parker, Meteorological survey of Mars, 1969–1984, *J. Geophys. Res.*, 95, 14,657–14,675, 1990.

Bell, J. F., III, R. V. Morris, and J. B. Adams, Thermally altered palagonitic tephra: A spectral and process analog to the soils and dust of Mars, *J. Geophys. Res.*, 98, 3373–3385, 1993.

Bell, J. F., III, W. M. Calvin, M. E. Ockert-Bell, D. Crisp, J. B. Pollack, and J. Spencer, Detection and monitoring of H_2O and CO_2 ice clouds on Mars, *J. Geophys. Res.*, 101, 9227–9237, 1996.

Bell, J. F., III, M. J. Wolff, P. B. James, R. T. Clancy, S. W. Lee, and L. J. Martin, Mars surface mineralogy from Hubble Space Telescope imaging during 1994–1995: Observations, calibration, and initial results, *J. Geophys. Res.*, 102, 9109–9123, 1997.

Christensen, P. R., Regional dust deposits on Mars: Physical properties, age, and history, *J. Geophys. Res.*, 91, 3533–3545, 1986.

Christensen, P. R., Global albedo variations on Mars: Implications for active aeolian transport, deposition, and erosion, *J. Geophys. Res.*, 93, 7611–7624, 1988.

Christensen, P. R., and H. J. Moore, The Martian surface layer, in *Mars*, edited by H. H. Kieffer et al., pp. 686–729, Univ. of Ariz. Press, Tucson, 1992.

Christensen, P. R., et al., Thermal Emission Spectrometer experiment: The Mars Observer Mission, *J. Geophys. Res.*, 97, 7719–7734, 1992.

Christensen, P. R., J. L. Bandfield, M. D. Smith, V. E. Hamilton, and R. N. Clark, Identification of a basaltic component on the Martian surface from Thermal Emission Spectrometer data, *J. Geophys. Res.*, 105, 9609–9621, 2000a.

Christensen, P. R., et al., Detection of crystalline hematite mineralization on Mars by the Thermal Emission Spectrometer: Evidence for near-surface water, *J. Geophys. Res.*, 105, 9623–9642, 2000b.

Christensen, P. R., J. L. Bandfield, V. E. Hamilton, D. A. Howard, M. D. Lane, J. L. Piatek, S. W. Ruff, and W. L. Stefanov, A thermal emission spectral library of rock forming minerals, *J. Geophys. Res.*, 105, 9735–9739, 2000c.

Christensen, P. R., et al., Mars Global Surveyor Thermal Emission Spectrometer experiment: Investigation description and surface science results, *J. Geophys. Res.*, 106, 23,823–23,871, 2001.

Clancy, R. T., A. W. Grossman, M. J. Wolff, P. B. James, D. J. Rudy, Y. N. Billawala, B. J. Sandor, S. W. Lee, and D. O. Muhleman, Water vapor saturation at low altitudes around Mars aphelion: A key to Mars climate?, *Icarus*, 122, 36–62, 1996.

Clancy, R. T., B. J. Sandor, M. J. Wolff, P. R. Christensen, M. D. Smith, J. C. Pearl, B. J. Conrath, and R. J. Wilson, An intercomparison of ground-based millimeter, MGS TES, and Viking atmospheric temperature measurements: Seasonal and interannual variability of temperatures and dust loading in the global Mars atmosphere, *J. Geophys. Res.*, 105, 9553–9571, 2000.

Clark, R. N., and T. M. Hoefen, Spectral feature mapping with Mars Global Surveyor thermal emission spectra: Mineralogic implications, *Bull. Am. Astro. Soc.*, 32, 1118, 2000.

Conel, J. E., Infrared emissivities of silicates: Experimental results and a cloudy atmosphere model of spectral emission from condensed particulate mediums, *J. Geophys. Res.*, 74, 1614–1634, 1969.

Conrath, B., R. Curran, R. Hanel, V. Kunde, W. Maguire, J. Pearl, J. Pirraglia, and J. Walker, Atmospheric and surface properties of Mars obtained by infrared spectroscopy on Mariner 9, *J. Geophys. Res.*, 78, 4267–4278, 1973.

Crisp, D., Infrared radiative transfer in the dust-free Martian atmosphere, *J. Geophys. Res.*, 95, 14,577–14,588, 1990.

Crisp, J., and M. J. Bartholomew, Mid-infrared spectroscopy of Pahala ash palagonite and implications for remote sensing studies of Mars, *J. Geophys. Res.*, 97, 14,691–14,699, 1992.

Curran, R. J., B. J. Conrath, R. A. Hanel, V. G. Kunde, and J. C. Pearl, Mars: Mariner 9 spectroscopic evidence for H_2O ice clouds, *Science*, 182, 381–383, 1973.

Dollfus, A., M. Deschamps, and J. R. Zimbelman, Soil texture and granulometry at the surface of Mars, *J. Geophys. Res.*, 98, 3413–3429, 1993.

Edgett, K. S., and M. C. Malin, New views of Mars eolian activity, materials, and surface properties: Three vignettes from the Mars Global Surveyor Mars Orbiter Camera, *J. Geophys. Res.*, 105, 1623–1650, 2000.

Emslie, A. G., and J. R. Aronson, Spectral reflectance and emittance of particulate materials, 1, Theory, *Appl. Opt.*, 12, 2563–2572, 1973.

Goody, R. M., and Y. L. Yung, *Atmospheric Radiation*, 519 pp., Oxford Univ. Press, New York, 1989.

Hamilton, V. E., Thermal Infrared Emission Spectroscopy of the Pyroxene Mineral Series and Pyroxene-bearing Lithologies, Ph.D. dissertation, Arizona State Univ., Arizona, 1998.

Hamilton, V. E., and P. R. Christensen, Determining the modal mineralogy of mafic and ultramafic igneous rocks using thermal emission spectroscopy, *J. Geophys. Res.*, 105, 9717–9733, 2000.

Hanel, R., et al., Investigation of the Martian environment by infrared spectroscopy on Mariner 9, *Icarus*, *17*, 423–442, 1972.

Hoefen, T. M., R. N. Clark, J. C. Pearl, and M. D. Smith, Unique spectral features in Mars Global Surveyor Thermal Emission Spectra: Implications for surface mineralogy in Nili Fossae, *Bull. Am. Astro. Soc.*, *32*, 1118, 2000.

Hunt, G. R., and R. K. Vincent, The behavior of spectral features in the infrared emission from particulate surfaces of various grain sizes, *J. Geophys. Res.*, *73*, 6039–6046, 1968.

Jakosky, B. M., and P. R. Christensen, Global duricrust on Mars: Analysis of remote sensing data, *J. Geophys. Res.*, *91*, 3547–3560, 1986.

Jakosky, B. M., and C. B. Farmer, The seasonal and global behavior of water vapor in the Mars atmosphere: Complete global results of the Viking atmospheric water detector experiment, *J. Geophys. Res.*, *87*, 2999–3019, 1982.

Johnson, J. R., P. R. Christensen, and P. G. Lucey, Dust coatings on basaltic rocks and implications for thermal infrared spectroscopy of Mars, *J. Geophys. Res.*, *107*(E6), 5035, doi:10.1029/2000JE001405, 2002.

Kieffer, H. H., J. S. C. Chase, E. Miner, G. Münch, and G. Neugebauer, Preliminary report on infrared radiometric measurements from Mariner 9 spacecraft, *J. Geophys. Res.*, *78*, 4291–4312, 1973.

Kieffer, H. H., T. Z. Martin, A. R. Peterfreund, B. M. Jakosky, E. D. Miner, and F. D. Palluconi, Thermal and albedo mapping of Mars during the Viking primary mission, *J. Geophys. Res.*, *82*, 4249–4292, 1977.

Kunde, V. G., and W. C. Maguire, Direct integration transmittance model, *J. Quant. Spec. Rad. Trans.*, *14*, 803–817, 1974.

Lane, M. D., Infrared optical constants of calcite and their relationship to particle size effects in thermal emission spectra of granular calcite, *J. Geophys. Res.*, *104*, 14,099–14,108, 1999.

Lane, M. D., and P. R. Christensen, Thermal infrared emission spectroscopy of salt minerals predicted for Mars, *Icarus*, *135*, 528–536, 1998.

Lyon, R. J. P., Analysis of rocks by spectral infrared emission (8–25 microns), *Econ. Geol.*, *60*, 715–736, 1965.

Maguire, W. C., Martian isotopic ratios and upper limits for possible minor constituents as derived from Mariner 9 infrared spectrometer data, *Icarus*, *32*, 85–97, 1977.

McAfee, J. M., and L. E. Kirkland, A model-independent correction of Mars thermal spectra near 7.8 mm for $CO^{16}O^{18}$ atmospheric absorption, in *Lunar Planet. Sci. XXXI*, abstract 1967 [CD-ROM], 2000.

McSween, H. Y., Jr., and K. Keil, Mixing relationships in the Martian regolith and the composition of globally homogeneous dust, *Geochim. Cosmochim. Acta*, *64*, 2155–2166, 2000.

Moersch, J. E., and P. R. Christensen, Thermal emission from particulate surfaces: A comparison of scattering models with measured spectra, *J. Geophys. Res.*, *100*, 7465–7477, 1995.

Moersch, J. E., T. Hayward, P. Nicholson, S. W. Squyres, J. V. Cleve, and P. R. Christensen, Identification of a 10 μm silicate absorption feature in the Acidalia region of Mars, *Icarus*, *126*, 183–196, 1997.

Morris, R. V., D. C. Golden, J. F. Bell III, H. V. J. Lauer, and J. B. Adams, Pigmenting agents in Martian soils: Inferences from spectral, Mössbauer, and magnetic properties of nanophase and other iron oxides in Hawaiian palagonitic soil PN-9, *Geochim. Cosmochim. Acta*, *57*, 4597–4609, 1993.

Morris, R. V., et al., Mineralogy, composition, and alteration of Mars Pathfinder rocks and soils: Evidence from multispectral, elemental, and magnetic data on terrestrial analogue, SNC meteorite, and pathfinder samples, *J. Geophys. Res.*, *105*, 1757–1817, 2000.

Morris, R. V., D. C. Golden, D. W. Ming, T. D. Shelfer, L. C. Jorgensen, and J. F. Bell III, Phyllosilicate-poor palagonitic dust from Mauna Kea Volcano (Hawaii): A mineralogical analogue for magnetic Martian dust?, *J. Geophys. Res.*, *106*, 5057–5083, 2001.

Mustard, J. F., and J. E. Hays, Effects of hyperfine particles on reflectance spectra from 0.3 to 25 μm, *Icarus*, *145*–163, 1997.

Mustard, J. F., S. Erard, J.-P. Bibring, J. W. Head, S. Hurtrez, Y. Langevin, C. M. Pieters, and C. J. Sotin, The surface of Syrtis Major: Composition of the volcanic substrate and mixing with altered dust and soil, *J. Geophys. Res.*, *98*, 3387–3400, 1993.

Pearl, J. C., M. D. Smith, B. J. Conrath, J. L. Bandfield, and P. R. Christensen, Observations of Martian ice clouds by the Mars Global Surveyor Thermal Emission Spectrometer: The first Martian year, *J. Geophys. Res.*, *106*, 12,325–12,338, 2001.

Pollack, J. B., et al., Thermal emission spectra of Mars (5.4–10.5 μm): Evidence for sulfates, carbonates, and hydrates, *J. Geophys. Res.*, *95*, 14,595–14,627, 1990.

Presley, M. A., and P. R. Christensen, Thermal conductivity measurements of particulate materials, 2, Results, *J. Geophys. Res.*, *102*, 6566–6651, 1997.

Ramsey, M. S., and P. R. Christensen, Mineral abundance determination: Quantitative deconvolution of thermal emission spectra, *J. Geophys. Res.*, *103*, 577–596, 1998.

Rothman, L. S., R. L. Hawkins, R. B. Watson, and R. R. Gamache, Energy levels, intensities, and linewidths of atmospheric carbon dioxide bands, *J. Quant. Spec. Rad. Trans.*, *48*, 537–566, 1992.

Ruff, S. W., and P. R. Christensen, Thermal-infrared spectral characteristics of Martian albedo features: Clues to composition, in *The Fifth International Conference on Mars*, abstract 6230 [CD-ROM], 1999.

Ruff, S. W., et al., Mars' "White Rock" lacks evidence of an aqueous origin: Results from Mars Global Surveyor, *J. Geophys. Res.*, *106*, 23,921–23,927, 2001.

Sagan, C., and J. B. Pollack, Windblown dust on Mars, *Nature*, *222*, 791–794, 1969.

Salisbury, J. W., The light and dark areas of Mars, *Icarus*, *5*, 291–298, 1966.

Salisbury, J. W., and A. Wald, The role of volume scattering in reducing spectral contrast of reststrahlen bands in spectra of powdered minerals, *Icarus*, *96*, 121–128, 1992.

Salisbury, J. W., and L. S. Walter, Thermal infrared (2.5–13.5 μm) spectroscopic remote sensing of igneous rock types on particulate planetary surfaces, *J. Geophys. Res.*, *94*, 9192–9202, 1989.

Salisbury, J. W., B. Hapke, and J. W. Eastes, Usefulness of weak bands in midinfrared remote sensing of particulate planetary surfaces, *J. Geophys. Res.*, *92*, 702–710, 1987.

Salisbury, J. W., D. M. D'Aria, and E. Jarosewich, Mid-infrared (2.5–13.5 um) reflectance spectra of powdered stony meteorites, *Icarus*, *92*, 280–297, 1991.

Salisbury, J. W., A. Basu, and E. M. Fischer, Thermal infrared spectra of lunar soils, *Icarus*, *130*, 125–139, 1997.

Singer, R. B., Spectral evidence for the mineralogy of high-albedo soils and dust on Mars, *J. Geophys. Res.*, *87*, 10,159–10,168, 1982.

Singer, R. B., T. B. McCord, R. N. Clark, J. B. Adams, and R. L. Huguenin, Mars surface composition from reflectance spectroscopy: A summary, *J. Geophys. Res.*, *84*, 8415–8426, 1979.

Smith, M. D., J. L. Bandfield, and P. R. Christensen, Separation of atmospheric and surface spectral features in Mars Global Surveyor Thermal Emission Spectrometer (TES) spectra, *J. Geophys. Res.*, *105*, 9589–9607, 2000a.

Smith, M. D., J. C. Pearl, B. J. Conrath, and P. R. Christensen, Mars Global Surveyor Thermal Emission Spectrometer (TES) observations of dust opacity during aerobraking and science phasing, *J. Geophys. Res.*, *105*, 9539–9552, 2000b.

Sullivan, R., P. Thomas, J. Veverka, M. Malin, and K. S. Edgett, Mass movement slope streaks imaged by the Mars Orbiter Camera, *J. Geophys. Res.*, *106*, 23,607–23,633, 2001.

Toon, O. B., J. B. Pollack, and C. Sagan, Physical properties of the particles comprising the Martian dust storm of 1971–1972, *Icarus*, *30*, 663–696, 1977.

Vincent, R. K., and G. R. Hunt, Infrared reflectance from mat surfaces, *Appl. Opt.*, *7*, 53–59, 1968.

Wald, A. E., and J. W. Salisbury, Thermal infrared directional emissivity of powdered quartz, *J. Geophys. Res.*, *100*, 24,665–24,675, 1995.

Wyatt, M. B., V. E. Hamilton, H. Y. McSween Jr., P. R. Christensen, and L. A. Taylor, Analysis of terrestrial and Martian volcanic compositions using thermal emission spectroscopy, 1, Determination of mineralogy, chemistry, and classification strategies, *J. Geophys. Res.*, *106*, 14,711–14,732, 2001.

Young, L. D. G., Transmission of CO_2 in the atmosphere of Venus for the spectral region near 7 microns, *Icarus*, *51*, 606–609, 1982.

———————

P. R. Christensen and S. W. Ruff, Mars Space Flight Facility, Department of Geological Sciences, Arizona State University, Box 876305, Tempe, AZ 85287-6305, USA. (ruff@tes.asu.edu)